ELSEVIER

Contents lists available at ScienceDirect

# Journal of Computational Physics

www.elsevier.com/locate/jcp



# Arbitrarily high-order linear energy stable schemes for gradient flow models



Yuezheng Gong<sup>a</sup>, Jia Zhao<sup>b</sup>, Qi Wang<sup>c,\*</sup>

- <sup>a</sup> College of Science, Nanjing University of Aeronautics and Astronautics, Nanjing 210016, China
- b Department of Mathematics & Statistics, Utah State University, Logan, UT 84322, USA
- <sup>c</sup> Department of Mathematics, University of South Carolina, Columbia, SC 29208, USA

#### ARTICLE INFO

#### Article history:

Received 22 October 2019 Received in revised form 15 May 2020 Accepted 27 May 2020 Available online 5 June 2020

#### Keywords:

Energy stable schemes Gradient flow models Runge-Kutta methods Linear high-order schemes Pseudo-spectral methods

#### ABSTRACT

We present a paradigm for developing arbitrarily high order, linear, unconditionally energy stable numerical algorithms for general gradient flow models. We apply the energy quadratization (EQ) technique to reformulate the gradient flow model into an equivalent one with a quadratic free energy and a modified mobility. For any positive integer k>0 and  $t_n=n\Delta t$ , where  $\Delta t$  is the time step size, we linearize the EQ-reformulated model in  $(t_n,t_{n+1}]$  through an extrapolation from numerical solutions already obtained in  $[0,t_n]$  so that the approximation error is in the order of  $O(\Delta t^k)$ . Then we employ an s-stage algebraically stable Runge-Kutta method to discretize the linearized model in  $(t_n,t_{n+1}]$ . For the spatial discretization, we use the Fourier pseudo-spectral method to match the order of accuracy in time. The resulting fully discrete scheme is linear, unconditionally energy stable, uniquely solvable, and can reach arbitrarily high order. Furthermore, we present a family of linear schemes based on prediction-correction methods to complement the new linear schemes. Some benchmark numerical examples are given to demonstrate the accuracy and efficiency of the schemes.

© 2020 Elsevier Inc. All rights reserved.

#### 1. Introduction

For many import phenomena in science and engineering, the corresponding processes are driven by minimizing the free energy or maximizing entropy through dissipative dynamics. Gradient flow models are usually used to investigate these phenomena. The generic form of a gradient flow model is given by

$$\frac{\partial}{\partial t}\Phi(\mathbf{x},t) = \mathcal{G}\frac{\delta F}{\delta \Phi}, \mathbf{x} \in \Omega \subset \mathbf{R}^n$$
(1.1)

with proper boundary conditions at  $\partial\Omega$ , where  $\Omega$  is the domain of the model. Here  $\Phi(\mathbf{x},t)$  is the thermodynamical variable,  $F[\Phi]$  is the free energy functional for the isothermal system (or entropy for the nonisothermal system), and  $\mathcal{G}$  is the mobility operator/matrix. The gradient flow model is thermodynamically consistent if it yields a positive entropy production or negative energy dissipation rate. The classical Allen-Cahn equation [4] and Cahn-Hilliard equation [5] are two examples of gradient flow models (1.1). Other gradient flow models include the molecular beam epitaxy model [12], the phase-field

<sup>\*</sup> Corresponding author at: Department of Mathematics, University of South Carolina, Columbia, SC 29208, USA. E-mail addresses: gongyuezheng@nuaa.edu.cn (Y. Gong), jia.zhao@usu.edu (J. Zhao), qwang@math.sc.edu (Q. Wang).

crystal model [15], the thermodynamically consistent dendritic growth model [45], the surfactant model [43], the diblock copolymer model [11] etc.

Most gradient flow models are nonlinear so that their analytical solutions are intractable. Hence, designing accurate, efficient, and stable algorithms to solve them becomes essential [16,18,40,44,47,54,55]. A numerical scheme that preserves the energy dissipation property is known as an energy stable scheme [16]. It has been shown that schemes that are not energy stable can lead to instability or oscillatory solutions [18]. This is because non-energy-stable schemes may introduce truncation errors that destroy the dissipative structure/property of the underlying equation numerically. Thus, developing energy stable numerical algorithms is necessary for accurately resolving dynamics of gradient flow models [25,27,29,38,55].

Over the years, development of numerical algorithms has been done primarily on a specific gradient flow model, exploiting its specific mathematical properties and structures. The noticeable ones include the Allen-Cahn and Cahn-Hilliard equation [2,8,10,13,14,16,25,26,30,40,46,49,53] as well as the molecular beam epitaxy model [7,9,17,31,33–36,52]. As a result, most numerical algorithms developed for a specific gradient flow model can hardly be applied to another gradient flow model with a different free energy and mobility. The status-quo did not change until the energy quadratization (EQ) approach was introduced a few years ago [50,55], which has proven to be applicable to general gradient flow models with no restrictions on the specific form of the mobility and free energy [21,51] (so long as the free energy is bounded below, which is required by the thermodynamical consistency). Based on the idea of EQ, the scalar auxiliary variable (SAV) approach was introduced later [39], where in each time step only linear systems with constant coefficients need to be solved. Several other extensions of EQ and SAV approaches have been explored further recently. For instance, regularization terms [6] and stabilization terms [48] are added, and the modified energy quadratization technique [28,32] are introduced to improve the EQ methodology. We notice that most existing schemes related to the EQ methodology are up to second-order accurate in time. Some higher-order ETD schemes have been introduced to solve the MBE model and Cahn-Hilliard models recently, but their theoretical proofs on energy stability are often missing. Shen et al. [38] remarked on the energy stability of higher-order BDF schemes using the SAV approach, but once again no rigorous theoretical proofs are given.

To develop high-order energy stable schemes, Shin et al. recently proposed a class of convex splitting Runge-Kutta (CSRK) methods for gradient flow models, but it requires many stages to reach third-order accuracy [41,42]. Akrivis et al. [1] proposed linear high-order energy-decaying methods for the Allen-Cahn and Cahn-Hilliard equations, based on the SAV and Runge-Kuta approach. Recently, Gong et al. [20,23,24] introduced arbitrarily high-order schemes to solve general gradient flow models by combining the methodology of energy quadratization with quadratic invariant Runge-Kutta (RK) methods. We note that the proposed high order schemes are fully nonlinear so that the solution existence and uniqueness of discretized systems are not guaranteed when the time step is large. Moreover, the implementation can be complicated compared to linear schemes. Often, it requires iterations at each time step, which adds up to the computational cost. Nevertheless, this seminal idea of combining RK methods with EQ methodology motivates us to explore an alternative approach to address the issue of nonlinearity.

In this paper, we propose a new paradigm for developing arbitrarily high order schemes that are unconditionally energy stable and linear. As a significant advance over our previous work, the newly proposed paradigm would result in linear schemes, while preserving unconditional energy stability. These newly proposed schemes bring in significant improvement in efficiency in numerical implementation and reduction in computational cost. First of all, as the schemes are all linear, only linear systems need to be solved at each time step. Therefore, they are easy to be implemented and computationally efficient. In addition, the existence and uniqueness of the numerical solutions can be guaranteed, independent of time steps. Namely, larger time steps can be applied so long as the accuracy requirement is met. This is, in fact, warranted by the existence of a unique solution and unconditionally energy stable. Combined with the benefits of the EQ method and the RK method, the newly proposed schemes can be applied to general gradient flow models. For illustration purposes, we solve the Cahn-Hilliard model and the molecular beam epitaxy model respectively in this study to demonstrate the effectiveness of some selected new schemes. To show their accuracy and efficiency, we also compare two proposed schemes with some existing schemes in the literature.

The rest of this paper is organized as follows. In Section 2, we briefly introduce the general gradient flow model and use the EQ method to reformulate it into an equivalent form. In Section 3, the arbitrarily high-order linear energy stable schemes are introduced to the reformulated gradient flow model with a quadratic free energy, and their energy stability and uniquely solvability are established. In Section 4, several numerical examples are shown to illustrate the power of the newly proposed, arbitrarily high order schemes. In the end, some concluding remarks are given.

#### 2. Gradient flow models and their EQ reformulation

In this section, we present the general gradient flow model firstly and then apply the energy quadratization technique to reformulate the model into an equivalent gradient flow form with a quadratic energy functional, a modified mobility matrix, and the corresponding energy dissipation law, which is called the EQ reformulated model. The EQ reformulation for this class of gradient flow models provides an elegant platform for developing arbitrarily high-order unconditionally energy stable schemes [20,24].

#### 2.1. Gradient flow model

Mathematically, the form of a general gradient flow model is given by [39,55]

$$\frac{\partial}{\partial t} \Phi(\mathbf{x}, t) = \mathcal{G} \frac{\delta F}{\delta \Phi}, \mathbf{x} \in \Omega, \tag{2.1}$$

where  $\Phi = (\phi_1, \dots, \phi_d)^T$  is the state variable vector,  $\mathcal{G}$  is the  $d \times d$  mobility matrix operator which can depend on  $\Phi$ , F is the free energy, and  $\frac{\delta F}{\delta \Phi}$  is the variational derivative of the free energy functional with respect to the state variable, known as the chemical potential. The triple  $(\Phi, \mathcal{G}, F)$  uniquely defines the gradient flow model. For (2.1) to be thermodynamically consistent, the time rate of change of the free energy must be non-increasing:

$$\frac{dF}{dt} = \left(\frac{\delta F}{\delta \Phi}, \frac{\partial \Phi}{\partial t}\right) = \left(\frac{\delta F}{\delta \Phi}, \mathcal{G}\frac{\delta F}{\delta \Phi}\right) \le 0,\tag{2.2}$$

where the inner product is defined by  $(\mathbf{f}, \mathbf{g}) = \sum_{i=1}^{d} \int_{\Omega} f_{i}g_{i}d\mathbf{x}$ ,  $\forall \mathbf{f}, \mathbf{g} \in \left(L^{2}(\Omega)\right)^{d}$ , which requires  $\mathcal{G}$  to be negative semi-definite.

The  $L^2$  norm is defined as  $\|\mathbf{f}\|_2 = \sqrt{(\mathbf{f}, \mathbf{f})}$ . Note that the energy dissipation law (2.2) holds only for suitable boundary conditions. Such boundary conditions include periodic boundary conditions and the other boundary conditions that make the boundary integrals resulted from the integration by parts vanish in the calculation of variational derivatives. In this paper, we limit our study to these boundary conditions.

## 2.2. Model reformulation using the EQ approach

We reformulate gradient flow model (2.1) by transforming the free energy into a quadratic form using nonlinear transformations. For the purpose of illustration, we assume the free energy is given by the following

$$F = \frac{1}{2}(\Phi, \mathcal{L}\Phi) + (f(\Phi, \nabla\Phi), 1), \tag{2.3}$$

where  $\mathcal{L}$  is a linear, self-adjoint, positive semi-definite operator (independent of  $\Phi$ ), and f is the bulk part of the free energy density, which has a lower bound. Then the free energy F can be rewritten into a quadratic form

$$\mathcal{F} = \frac{1}{2}(\Phi, \mathcal{L}\Phi) + \|q\|^2 - C|\Omega|,\tag{2.4}$$

by introducing an auxiliary variable  $q = \sqrt{f(\Phi, \nabla \Phi) + C}$ , where C is a positive constant large enough to make q a real-value function for all  $\Phi(\mathbf{x}, t), \mathbf{x} \in \Omega$ .

We denote  $g[\Phi] = \sqrt{f(\Phi, \nabla \Phi) + C}$ . Then model (2.1) can be reformulated into the following equivalent system

$$\begin{cases}
\Phi_t = \mathcal{G}\left(\mathcal{L}\Phi + 2q\frac{\partial g}{\partial \Phi} - \nabla \cdot \left(2q\frac{\partial g}{\partial \nabla \Phi}\right)\right), \\
q_t = \frac{\partial g}{\partial \Phi} \cdot \Phi_t + \frac{\partial g}{\partial \nabla \Phi} \cdot \nabla \Phi_t,
\end{cases} (2.5)$$

with consistent initial conditions

$$\Phi(\mathbf{x},0) = \Phi_0(\mathbf{x}), \quad q(\mathbf{x},0) = \sqrt{f(\Phi_0(\mathbf{x}), \nabla \Phi_0(\mathbf{x})) + C}.$$
 (2.6)

It is readily to prove that reformulated system (2.5) preserves the following energy dissipation law

$$\frac{d\mathcal{F}}{dt} = \left(\mathcal{L}\Phi + 2q\frac{\partial g}{\partial \Phi} - \nabla \cdot \left(2q\frac{\partial g}{\partial \nabla \Phi}\right), \mathcal{G}\left(\mathcal{L}\Phi + 2q\frac{\partial g}{\partial \Phi} - \nabla \cdot \left(2q\frac{\partial g}{\partial \nabla \Phi}\right)\right)\right) \le 0. \tag{2.7}$$

We emphasis that, in the continuous level, the EQ-reformulated form (2.5) is equivalent to the original gradient flow system (2.1), and their energy dissipation laws in (2.7) and (2.2) are equivalent as well.

We introduce

$$\mathbf{u} = (\Phi, q)^T \tag{2.8}$$

and recast the system (2.5) into a compact gradient flow form

$$\mathbf{u}_{t} = \mathcal{M} \frac{\delta \mathcal{F}}{\delta \mathbf{u}},\tag{2.9}$$

with a modified mobility operator

$$\mathcal{M} = \begin{pmatrix} 1 \\ \frac{\partial g}{\partial \Phi} + \frac{\partial g}{\partial \nabla \Phi} \cdot \nabla \end{pmatrix} \mathcal{G} \left( 1, \frac{\partial g}{\partial \Phi} - \nabla \cdot \frac{\partial g}{\partial \nabla \Phi} \right). \tag{2.10}$$

The energy dissipation law given in (2.7) is recast into

$$\frac{d\mathcal{F}}{dt} = \left(\frac{\delta \mathcal{F}}{\delta \mathbf{u}}, \mathcal{M} \frac{\delta \mathcal{F}}{\delta \mathbf{u}}\right) \le 0. \tag{2.11}$$

Since the EQ-reformulated form in (2.5) has a quadratic free energy, we next discuss how to devise linear high-order energy stable schemes for it, which in turn solves the original gradient flow system (2.1).

#### 3. High-order linear energy stable schemes

In this section, we first derive a high-precision linear gradient-flow system to approximate EQ-reformulated model (2.5) up to  $t_n = n\Delta t$ , where  $\Delta t$  is the time step. In particular, we require that the corresponding energy dissipation law is inherited by the approximate linear gradient-flow system. Then the algebraically stable RK method [3] is applied to the resulting linear gradient-flow system to develop a class of linear semi-discrete schemes in time. We name the schemes linear energy quadratized Runge-Kutta (LEQRK) schemes. In order to improve accuracy and stability, a prediction-correction technique is proposed for the LEQRK schemes, leading to the LEQRK-PC method. These new algorithms are linear, unconditionally energy stable, and can be devised at any desired order in time.

#### 3.1. LEQRK schemes

Assuming numerical solutions of  $\Phi$  up to  $t \le t_n$  have been obtained, we then solve system (2.5) in  $t \in (t_n, t_{n+1}]$  approximately. We utilize the numerical solutions of  $\Phi$  at  $t \le t_n$  to obtain its interpolating polynomial approximation denoted by  $\Phi_N(t)$ . Then we approximate model (2.5) in  $(t_n, t_{n+1}]$  using the following linear, variable coefficient gradient flow system

$$\begin{cases}
\Phi_{t} = \mathcal{G}\left(\mathcal{L}\Phi + 2q\frac{\partial g_{N}}{\partial \Phi} - \nabla \cdot \left(2q\frac{\partial g_{N}}{\partial \nabla \Phi}\right)\right), \\
q_{t} = \frac{\partial g_{N}}{\partial \Phi} \cdot \Phi_{t} + \frac{\partial g_{N}}{\partial \nabla \Phi} \cdot \nabla \Phi_{t},
\end{cases}$$
(3.1)

where  $\mathcal{G} = \mathcal{G}(\Phi_N(\mathbf{x},t))$ ,  $\frac{\partial g_N}{\partial \Phi} = \frac{\partial g}{\partial \Phi}[\Phi_N(\mathbf{x},t)]$  and  $\frac{\partial g_N}{\partial \nabla \Phi} = \frac{\partial g}{\partial \nabla \Phi}[\Phi_N(\mathbf{x},t)]$  are functions of  $\Phi_n(\mathbf{x},t)$  and independent of  $\Phi$ . The linear gradient flow system (3.1) satisfies the following energy dissipation law

$$\frac{d\mathcal{F}}{dt} = \left(\mathcal{L}\Phi + 2q\frac{\partial g_N}{\partial \Phi} - \nabla \cdot \left(2q\frac{\partial g_N}{\partial \nabla \Phi}\right), \mathcal{G}\left(\mathcal{L}\Phi + 2q\frac{\partial g_N}{\partial \Phi} - \nabla \cdot \left(2q\frac{\partial g_N}{\partial \nabla \Phi}\right)\right)\right) \le 0. \tag{3.2}$$

Applying a s-stage RK method for the linear system (3.1), we obtain the following LEQRK scheme. To simplify the presentation, we present the scheme with a constant mobility  $\mathcal{G}$ . For cases with variable mobility operators, please refer to Remark 3.2 given below. We also abbreviate  $\Phi(\mathbf{x},t)$  into  $\Phi(t)$  for simplicity since this schemes are semi-discrete in time.

**Scheme 3.1** (s-stage LEQRK Scheme). Let  $b_i$ ,  $a_{ij}$  (i,  $j=1,\cdots,s$ ) be real numbers and let  $c_i=\sum\limits_{j=1}^s a_{ij}$ . For given  $(\Phi^n,q^n)$  and  $\Phi_N(t_n+c_i\Delta t)$ ,  $\forall i$ , the following intermediate values are first calculated by

$$\begin{cases}
\Phi_{i}^{n} = \Phi^{n} + \Delta t \sum_{j=1}^{s} a_{ij} k_{j}^{n}, \\
Q_{i}^{n} = q^{n} + \Delta t \sum_{j=1}^{s} a_{ij} l_{j}^{n}, \\
k_{i}^{n} = \mathcal{G} \left( \mathcal{L} \Phi_{i}^{n} + 2 Q_{i}^{n} \left( \frac{\partial g}{\partial \Phi} \right)_{i}^{n,*} - \nabla \cdot \left( 2 Q_{i}^{n} \left( \frac{\partial g}{\partial \nabla \Phi} \right)_{i}^{n,*} \right) \right), \\
l_{i}^{n} = \left( \frac{\partial g}{\partial \Phi} \right)_{i}^{n,*} \cdot k_{i}^{n} + \left( \frac{\partial g}{\partial \nabla \Phi} \right)_{i}^{n,*} \cdot \nabla k_{i}^{n},
\end{cases} (3.3)$$

where  $\left(\frac{\partial g}{\partial \Phi}\right)_i^{n,*} = \frac{\partial g}{\partial \Phi}[\Phi_N(t_n + c_i\Delta t)]$  and  $\left(\frac{\partial g}{\partial \nabla \Phi}\right)_i^{n,*} = \frac{\partial g}{\partial \nabla \Phi}[\Phi_N(t_n + c_i\Delta t)]$ . Then  $(\Phi^{n+1}, q^{n+1})$  is updated via

$$\Phi^{n+1} = \Phi^n + \Delta t \sum_{i=1}^s b_i k_i^n, \tag{3.4}$$

$$q^{n+1} = q^n + \Delta t \sum_{i=1}^s b_i l_i^n.$$
(3.5)

**Definition 3.1** (Algebraically stable RK method [3]). Denote a symmetric matrix  $\mathbf{M}$  with the elements  $\mathbf{M}_{ij} = b_i a_{ij} + b_j a_{ji} - b_i b_j$ . A RK method is said to be algebraically stable if its RK coefficients satisfy stability condition

$$b_i \ge 0, \ \forall i = 1, 2, \dots, s, \quad \text{and } \mathbf{M} \text{ is positive semi-definite.}$$
 (3.6)

Next, we show that the algebraically stable LEQRK scheme is unconditionally energy stable.

**Theorem 3.1.** The LEQRK scheme with their RK coefficients satisfying stability condition (3.6) is unconditionally energy stable, i.e., it satisfies

$$\mathcal{F}^{n+1} \le \mathcal{F}^n,$$
where  $\mathcal{F}^n = \frac{1}{2}(\Phi^n, \mathcal{L}\Phi^n) + \|q^n\|^2 - C|\Omega|.$ 
(3.7)

**Proof.** Denoting  $\Phi^{n+1} = \Phi^n + \Delta t \sum_{i=1}^s b_i k_i^n$  and noticing that operator  $\mathcal{L}$  is linear and self-adjoint, we have

$$\frac{1}{2}(\Phi^{n+1}, \mathcal{L}\Phi^{n+1}) - \frac{1}{2}(\Phi^n, \mathcal{L}\Phi^n) = \Delta t \sum_{i=1}^s b_i(k_i^n, \mathcal{L}\Phi^n) + \frac{\Delta t^2}{2} \sum_{i,j=1}^s b_i b_j(k_i^n, \mathcal{L}k_j^n). \tag{3.8}$$

Applying  $\Phi^n = \Phi_i^n - \Delta t \sum_{j=1}^s a_{ij} k_j^n$  to the right of (3.8), we deduce

$$\frac{1}{2}(\Phi^{n+1}, \mathcal{L}\Phi^{n+1}) - \frac{1}{2}(\Phi^n, \mathcal{L}\Phi^n) = \Delta t \sum_{i=1}^s b_i(k_i^n, \mathcal{L}\Phi_i^n) - \frac{\Delta t^2}{2} \sum_{i,j=1}^s \mathbf{M}_{ij}(k_i^n, \mathcal{L}k_j^n), \tag{3.9}$$

where  $\sum_{i,j=1}^{s} b_i a_{ij} (k_i^n, \mathcal{L} k_j^n) = \sum_{i,j=1}^{s} b_j a_{ji} (k_i^n, \mathcal{L} k_j^n)$  and  $\mathbf{M}_{ij} = b_i a_{ij} + b_j a_{ji} - b_i b_j$  are used. Note that  $\mathcal{L}$  can be denoted as  $\mathcal{L} = \mathcal{A}^* \mathcal{A}$ , where  $\mathcal{A}$  is a linear operator and  $\mathcal{A}^*$  is the adjoint operator of  $\mathcal{A}$ . Since  $\mathbf{M}$  is positive semi-definite, we have

$$\sum_{i=1}^{s} \mathbf{M}_{ij}(k_i^n, \mathcal{L}k_j^n) = \sum_{i=1}^{s} \mathbf{M}_{ij}(\mathcal{A}k_i^n, \mathcal{A}k_j^n) \ge 0.$$

$$(3.10)$$

Combining eqs. (3.9) and (3.10) leads to

$$\frac{1}{2}(\Phi^{n+1}, \mathcal{L}\Phi^{n+1}) - \frac{1}{2}(\Phi^{n}, \mathcal{L}\Phi^{n}) \le \Delta t \sum_{i=1}^{s} b_{i}(k_{i}^{n}, \mathcal{L}\Phi_{i}^{n}). \tag{3.11}$$

Similarly, we have

$$\|q^{n+1}\|^2 - \|q^n\|^2 \le 2\Delta t \sum_{i=1}^s b_i(l_i^n, Q_i^n). \tag{3.12}$$

Adding (3.11) and (3.12) and noticing that  $l_i^n = \left(\frac{\partial g}{\partial \Phi}\right)_i^{n,*} \cdot k_i^n + \left(\frac{\partial g}{\partial \nabla \Phi}\right)_i^{n,*} \cdot \nabla k_i^n$ , we obtain

$$\mathcal{F}^{n+1} - \mathcal{F}^{n} \leq \Delta t \sum_{i=1}^{s} b_{i} \left( \mathcal{L} \Phi_{i}^{n} + 2Q_{i}^{n} \left( \frac{\partial g}{\partial \Phi} \right)_{i}^{n,*} - \nabla \cdot \left( 2Q_{i}^{n} \left( \frac{\partial g}{\partial \nabla \Phi} \right)_{i}^{n,*} \right), k_{i}^{n} \right). \tag{3.13}$$

Substituting  $k_i^n = \mathcal{G}\left(\mathcal{L}\Phi_i^n + 2Q_i^n\left(\frac{\partial g}{\partial \Phi}\right)_i^{n,*} - \nabla \cdot \left(2Q_i^n\left(\frac{\partial g}{\partial \nabla \Phi}\right)_i^{n,*}\right)\right)$  in (3.13) and noticing the negative semi-definite property of  $\mathcal{G}$  and  $b_i \geq 0$ ,  $\forall i$ , we arrive at  $\mathcal{F}^{n+1} - \mathcal{F}^n \leq 0$ . This completes the proof.  $\square$ 

**Remark 3.1.** Note that the Gauss method is a special kind of algebraically stable RK method, whose RK coefficients satisfy M = 0. Thus the Gauss method preserves the discrete energy dissipation law exactly:

$$\mathcal{F}^{n+1} - \mathcal{F}^{n} = \Delta t \sum_{i=1}^{s} b_{i} \left( \mathcal{L} \Phi_{i}^{n} + 2 Q_{i}^{n} \left( \frac{\partial g}{\partial \Phi} \right)_{i}^{n,*} - \nabla \cdot \left( 2 Q_{i}^{n} \left( \frac{\partial g}{\partial \nabla \Phi} \right)_{i}^{n,*} \right), k_{i}^{n} \right) \leq 0.$$
(3.14)

**Remark 3.2.** For the variable mobility operator  $\mathcal{G}[\Phi]$ , we will replace  $\mathcal{G}$  in (3.3) by  $\mathcal{G}[\Phi_N(t_n + c_i \Delta t)]$  to obtain the discrete scheme, which is linear and energy stable.

**Remark 3.3.** After appropriate spatial discretization that satisfies the discrete integration-by-parts formula (see [21,22] for details), the algebraically stable LEQRK scheme naturally leads to a fully discrete energy stable scheme. In this paper, we employ the Fourier pseudo-spectral method for spatial discretization. We omit the details here due to save space. Interested readers are referred to our earlier work [21,24] for details.

Next, we discuss solvability of the resulting fully discrete scheme.

**Theorem 3.2.** If RK coefficient matrix  $\mathbf{A} = (a_{ij})$  is positive semi-definite and mobility operator  $\mathcal{G}$  satisfies  $\mathcal{G} = -\mathcal{B}^*\mathcal{B}$ , the fully discrete scheme derived by applying the Fourier pseudo-spectral method to Scheme 3.1 is uniquely solvable.

**Proof.** Without loss of generality, we still use the notations  $\mathcal{G}$ ,  $\mathcal{L}$  and  $\nabla$  to denote the corresponding discrete operators in the fully discrete scheme. We consider the homogeneous linear equation system of (3.3)

$$\begin{cases}
\Phi_{i}^{n} = \Delta t \sum_{j=1}^{s} a_{ij} k_{j}^{n}, \\
Q_{i}^{n} = \Delta t \sum_{j=1}^{s} a_{ij} l_{j}^{n}, \\
k_{i}^{n} = \mathcal{G} \left( \mathcal{L} \Phi_{i}^{n} + 2 Q_{i}^{n} \left( \frac{\partial g}{\partial \Phi} \right)_{i}^{n,*} - \nabla \cdot \left( 2 Q_{i}^{n} \left( \frac{\partial g}{\partial \nabla \Phi} \right)_{i}^{n,*} \right) \right), \\
l_{i}^{n} = \left( \frac{\partial g}{\partial \Phi} \right)_{i}^{n,*} \cdot k_{i}^{n} + \left( \frac{\partial g}{\partial \nabla \Phi} \right)_{i}^{n,*} \cdot \nabla k_{i}^{n},
\end{cases} (3.15)$$

where  $\Phi_i^n$ ,  $Q_i^n$ ,  $k_i^n$ ,  $l_i^n$  are unknown. To prove unique solvability of the fully discrete scheme, we need to prove that the homogeneous linear equation system (3.15) admits only a zero solution.

Computing the discrete inner product of the third equation in (3.15) with  $\mathcal{L}\Phi_i^n + 2Q_i^n \left(\frac{\partial g}{\partial \Phi}\right)_i^{n,*} - \nabla \cdot \left(2Q_i^n \left(\frac{\partial g}{\partial \nabla \Phi}\right)_i^{n,*}\right)$  and sum over i, we deduce from (3.15)

$$\Delta t \sum_{i,i=1}^{s} a_{ij} (\mathcal{A} k_i^n, \mathcal{A} k_j^n) + 2\Delta t \sum_{i,j=1}^{s} a_{ij} (l_i^n, l_j^n) + \sum_{i=1}^{s} \left\| \mathcal{B} \left( \mathcal{L} \Phi_i^n + 2 Q_i^n \left( \frac{\partial g}{\partial \Phi} \right)_i^{n,*} - \nabla \cdot \left( 2 Q_i^n \left( \frac{\partial g}{\partial \nabla \Phi} \right)_i^{n,*} \right) \right) \right\|^2 = 0,$$

where  $\mathcal{G} = -\mathcal{B}^*\mathcal{B}$  and  $\mathcal{L} = \mathcal{A}^*\mathcal{A}$  are used. Since  $\mathbf{A} = (a_{ij})$  is positive semi-definite, which implies that the first two terms of the above equation are nonnegative, we have

$$\mathcal{B}\left(\mathcal{L}\Phi_{i}^{n}+2Q_{i}^{n}\left(\frac{\partial g}{\partial \Phi}\right)_{i}^{n,*}-\nabla\cdot\left(2Q_{i}^{n}\left(\frac{\partial g}{\partial \nabla \Phi}\right)_{i}^{n,*}\right)\right)=0,\quad\forall i,$$
(3.16)

which leads to

$$\mathcal{G}\left(\mathcal{L}\Phi_{i}^{n}+2Q_{i}^{n}\left(\frac{\partial g}{\partial \Phi}\right)_{i}^{n,*}-\nabla\cdot\left(2Q_{i}^{n}\left(\frac{\partial g}{\partial \nabla \Phi}\right)_{i}^{n,*}\right)\right)=0,\quad\forall i.$$

Therefore, according to (3.15), we arrive at

$$k_i^n = 0, \quad l_i^n = 0, \quad \Phi_i^n = 0, \quad Q_i^n = 0, \quad \forall i.$$
 (3.18)

This completes the proof.  $\Box$ 

**Theorem 3.3.** If diagonally implicit RK coefficients satisfy  $a_{ii} > 0$ , then the fully discrete scheme derived by applying the Fourier pseudo-spectral method to Scheme 3.1 is uniquely solvable.

**Proof.** For the diagonally implicit RK (DIRK) scheme, we solve  $\Phi_i^n$ ,  $Q_i^n$ ,  $k_i^n$ ,  $l_i^n$  in turn from i = 1 to s. Therefore, we here consider the following homogeneous linear equation system

$$\begin{cases}
\Phi_{i}^{n} = \Delta t a_{ii} k_{i}^{n}, \\
Q_{i}^{n} = \Delta t a_{ii} l_{i}^{n}, \\
k_{i}^{n} = \mathcal{G} \left( \mathcal{L} \Phi_{i}^{n} + 2 Q_{i}^{n} \left( \frac{\partial g}{\partial \Phi} \right)_{i}^{n,*} - \nabla \cdot \left( 2 Q_{i}^{n} \left( \frac{\partial g}{\partial \nabla \Phi} \right)_{i}^{n,*} \right) \right), \\
l_{i}^{n} = \left( \frac{\partial g}{\partial \Phi} \right)_{i}^{n,*} \cdot k_{i}^{n} + \left( \frac{\partial g}{\partial \nabla \Phi} \right)_{i}^{n,*} \cdot \nabla k_{i}^{n},
\end{cases} (3.19)$$

where  $\Phi_i^n$ ,  $Q_i^n$ ,  $k_i^n$ ,  $l_i^n$  are unknown. To prove unique solvability of the fully discrete scheme, we need to prove that homogeneous linear equation system (3.19) admits only a zero solution.

Similar to the proof of Theorem 3.2, we have

$$\begin{split} & \Delta t a_{ii} \|\mathcal{A} k_i^n\|^2 + 2\Delta t a_{ii} \|l_i^n\|^2 \\ &= \left( \mathcal{L} \Phi_i^n + 2Q_i^n \left( \frac{\partial g}{\partial \Phi} \right)_i^{n,*} - \nabla \cdot \left( 2Q_i^n \left( \frac{\partial g}{\partial \nabla \Phi} \right)_i^{n,*} \right), \mathcal{G} \left( \mathcal{L} \Phi_i^n + 2Q_i^n \left( \frac{\partial g}{\partial \Phi} \right)_i^{n,*} - \nabla \cdot \left( 2Q_i^n \left( \frac{\partial g}{\partial \nabla \Phi} \right)_i^{n,*} \right) \right) \right) \\ &\leq 0, \end{split}$$

which leads to

$$\mathcal{A}k_i^n = 0, \quad l_i^n = 0. \tag{3.20}$$

Combining (3.19) and (3.20), we deduce in turn

$$l_i^n = 0, \quad Q_i^n = 0, \quad \mathcal{L}k_i^n = 0, \quad \mathcal{L}\Phi_i^n = 0, \quad k_i^n = 0.$$
 (3.21)

This completes the proof.  $\Box$ 

**Remark 3.4.** In this paper, we give examples in two 4th-order algebraically stable RK methods, i.e., Gauss4th and DIRK4th given by the following Butcher tables, respectively,

with  $\sigma = \cos(\pi/18)/\sqrt{3} + 1/2$ ,  $\mu = 1/(6(2\sigma - 1)^2)$ . We note that Gauss4th and DIRK4th satisfy the conditions in Theorem 3.2 and Theorem 3.3, respectively. Therefore, after an appropriate spatial discretization, the LEQRK schemes equipped with Gauss4th or DIRK4th are uniquely solvable.

**Remark 3.5.** Noticing that  $\Phi_i^m$  approximates  $\Phi(t_m+c_i\Delta t)$ , we can choose the time nodes  $t_m$ ,  $t_m+c_i\Delta t$  (m< n) and  $t_n$  as the interpolation points to obtain the interpolation polynomial  $\Phi_N(t)$ . However, too many interpolation points will cause the interpolation polynomial to be highly oscillating, which may make  $\Phi_N(t_n+c_i\Delta t)$  an inaccurate extrapolation for  $\Phi(t_n+c_i\Delta t)$ . Therefore, we only take  $t_{n-1}$ ,  $t_{n-1}+c_i\Delta t$ ,  $\forall i$  and  $t_n$  as the interpolation points in this paper. For example, for the Gauss4th method, we choose the interpolation points  $(t_{n-1},\Phi^{n-1})$ ,  $(t_{n-1}+c_1\Delta t,\Phi_1^{n-1})$ ,  $(t_{n-1}+c_2\Delta t,\Phi_2^{n-1})$ ,  $(t_n,\Phi^n)$  and obtain the corresponding interpolation polynomial

$$\begin{split} \Phi_N(t_{n-1}+s\Delta t) &= \frac{(s-c_1)(s-c_2)(s-1)}{-c_1c_2} \Phi^{n-1} + \frac{s(s-c_2)(s-1)}{c_1(c_1-c_2)(c_1-1)} \Phi_1^{n-1} \\ &+ \frac{s(s-c_1)(s-1)}{c_2(c_2-c_1)(c_2-1)} \Phi_2^{n-1} + \frac{s(s-c_1)(s-c_2)}{(1-c_1)(1-c_2)} \Phi^n, \end{split}$$

where  $c_1 = 1/2 - \sqrt{3}/6$  and  $c_2 = 1/2 + \sqrt{3}/6$ . Thus we have

$$\Phi_N(t_n + c_1 \Delta t) = (2\sqrt{3} - 4)\Phi^{n-1} + (7\sqrt{3} - 11)\Phi_1^{n-1} + (6 - 5\sqrt{3})\Phi_2^{n-1} + (10 - 4\sqrt{3})\Phi^n, \tag{3.22}$$

$$\Phi_N(t_n + c_2 \Delta t) = -(2\sqrt{3} + 4)\Phi^{n-1} + (6 + 5\sqrt{3})\Phi_1^{n-1} - (7\sqrt{3} + 11)\Phi_2^{n-1} + (10 + 4\sqrt{3})\Phi^n.$$
(3.23)

Replacing n with n-1 in the first equation of (3.3) and (3.4), then we deduce

$$\Phi^{n} = \Phi^{n-1} - \sqrt{3}\Phi_{1}^{n-1} + \sqrt{3}\Phi_{2}^{n-1}. \tag{3.24}$$

According to (3.22)-(3.24), we obtain

$$\Phi_N(t_n + c_1 \Delta t) = (6 - 2\sqrt{3})\Phi^{n-1} + (1 - 3\sqrt{3})\Phi_1^{n-1} + (5\sqrt{3} - 6)\Phi_2^{n-1}, \tag{3.25}$$

$$\Phi_N(t_n + c_2 \Delta t) = (6 + 2\sqrt{3})\Phi^{n-1} - (5\sqrt{3} + 6)\Phi_1^{n-1} + (1 + 3\sqrt{3})\Phi_2^{n-1}. \tag{3.26}$$

Note that if we take  $t_{n-1}$ ,  $t_{n-1} + c_i \Delta t$  (i = 1, 2) as the interpolation points, we can also derive (3.25)-(3.26), which implies that the LEQRK scheme derived by the Gauss4th method and the interpolations (3.22)-(3.23) or (3.25)-(3.26) may achieve third order accuracy.

#### 3.2. LEORK-PC schemes

To improve accuracy as well as stability of Scheme 3.1, we propose a prediction-correction scheme motivated by the previous works in [19,24,37]. Employing the prediction-correction strategy to Scheme 3.1, we obtain the following prediction-correction method:

**Scheme 3.2** (s-stage LEQRK-PC scheme). Let  $b_i$ ,  $a_{ij}$   $(i, j = 1, \dots, s)$  be real numbers and let  $c_i = \sum_{j=1}^s a_{ij}$ . For given  $(\Phi^n, q^n)$  and  $\Phi_N(t_n + c_i \Delta t)$ ,  $Q_N(t_n + c_i \Delta t)$ ,  $\forall i$ , the following intermediate values are first calculated by the following prediction-correction strategy

1. Prediction: we set  $\Phi_i^{n,0} = \Phi_N(t_n + c_i \Delta t)$ ,  $Q_i^{n,0} = Q_N(t_n + c_i \Delta t)$ . Let M > 0 be a given integer. For m = 0 to M - 1, we compute  $\Phi_i^{n,m+1}$ ,  $k_i^{n,m+1}$ ,  $l_i^{n,m+1}$ ,  $Q_i^{n,m+1}$  using

$$\begin{cases} \Phi_{i}^{n,m+1} = \Phi^{n} + \Delta t \sum_{j=1}^{s} a_{ij} k_{j}^{n,m+1}, \\ k_{i}^{n,m+1} = \mathcal{G}\left(\mathcal{L}\Phi_{i}^{n,m+1} + 2Q_{i}^{n,m} \frac{\partial g}{\partial \Phi} [\Phi_{i}^{n,m}] - \nabla \cdot \left(2Q_{i}^{n,m} \frac{\partial g}{\partial \nabla \Phi} [\Phi_{i}^{n,m}]\right)\right), & i = 1, \dots, s. \\ l_{i}^{n,m+1} = \frac{\partial g}{\partial \Phi} [\Phi_{i}^{n,m+1}] \cdot k_{i}^{n,m+1} + \frac{\partial g}{\partial \nabla \Phi} [\Phi_{i}^{n,m+1}] \cdot \nabla k_{i}^{n,m+1}, \\ Q_{i}^{n,m+1} = q^{n} + \Delta t \sum_{j=1}^{s} a_{ij} l_{j}^{n,m+1}, \end{cases}$$

$$(3.27)$$

 $If\max_i \|\Phi_i^{n,m+1} - \Phi_i^{n,m}\|_{\infty} < TOL, \ we \ stop \ the \ iteration \ and \ set \ \Phi_i^{n,*} = \Phi_i^{n,m+1}; \ otherwise, \ we \ set \ \Phi_i^{n,*} = \Phi_i^{n,M}.$ 

2. Correction: for the predicted  $\Phi_i^{n,*}$ , we compute the intermediate values  $\Phi_i^n$ ,  $Q_i^n$ ,  $k_i^n$ ,  $l_i^n$  via

$$\begin{cases} \Phi_{i}^{n} = \Phi^{n} + \Delta t \sum_{j=1}^{s} a_{ij} k_{j}^{n}, \\ Q_{i}^{n} = q^{n} + \Delta t \sum_{j=1}^{s} a_{ij} l_{j}^{n}, \\ k_{i}^{n} = \mathcal{G} \left( \mathcal{L} \Phi_{i}^{n} + 2 Q_{i}^{n} \frac{\partial g}{\partial \Phi} [\Phi_{i}^{n,*}] - \nabla \cdot \left( 2 Q_{i}^{n} \frac{\partial g}{\partial \nabla \Phi} [\Phi_{i}^{n,*}] \right) \right), \\ l_{i}^{n} = \frac{\partial g}{\partial \Phi} [\Phi_{i}^{n,*}] \cdot k_{i}^{n} + \frac{\partial g}{\partial \nabla \Phi} [\Phi_{i}^{n,*}] \cdot \nabla k_{i}^{n}, \end{cases}$$

$$(3.28)$$

Then  $(\Phi^{n+1}, q^{n+1})$  is updated via

$$\Phi^{n+1} = \Phi^n + \Delta t \sum_{i=1}^{s} b_i k_i^n, \tag{3.29}$$

$$q^{n+1} = q^n + \Delta t \sum_{i=1}^s b_i l_i^n. {(3.30)}$$

**Remark 3.6.** Note that  $Q_N(t)$  in Scheme 3.2 denotes the interpolation polynomial of q. If we take  $\Phi_N(t) = \Phi^n$ ,  $Q_N(t) = q^n$ , then Scheme 3.1 reduces to first order while Scheme 3.2 with an appropriate prediction can achieve the desired high order. In other words, when accuracy of the interpolation is low, Scheme 3.1 has low order accuracy, while Scheme 3.2 with an appropriate prediction can improve the accuracy. In numerical computations, we will apply Scheme 3.2 to figure out the necessary initial information. In addition, when linear system (3.27) is of constant coefficients, it can be readily solved by using the fast Fourier transform (FFT).

If one skips the prediction step by choosing M=0, Scheme 3.2 reduces to Scheme 3.1. If M is large enough, the LEQRK-PC scheme approximates the IEQ-RK scheme proposed in [20]. There is no theoretical result on the choice of iteration step M. From our numerical experience, several iteration steps such as  $M \le 5$  would improve the accuracy noticeably. Similar to Scheme 3.1, we can also establish energy stability and solvability for the LEQRK-PC scheme, which is omitted here to save space.

Although reformulated system (2.5) with initial condition (2.6) is equivalent to the original model given in (2.1) in the continuum level, the proposed schemes here uses the spatially discretized, quadratized energy functional given in (2.4), instead of the original energy given in (2.3). However, we note that the discrete version of (2.4) is a high-order approximation of (2.3) when high order schemes are used.

We point out that when the time step is large, extrapolation  $\Phi_N(t)$  and  $Q_N(t)$  may not be accurate. In practice, for s-stage LEQRK-PC Scheme 3.2, we set  $\Phi_i^{n,0} = \Phi^n$  and  $Q_i^{n,0} = q^n$  as an initial guess in the prediction step to make the scheme more accurate. This doesn't affect the order of accuracy of the s-stage LEQRK-PC Scheme 3.2 when M is large.

**Remark 3.7.** Recently, Akrivis et al. [1] developed a new class of linear high-order energy-decaying methods for the Allen-Cahn and Cahn-Hilliard equations, based on the SAV approach and the extrapolated, linearized Runge-Kutta methods. They proved the convergence of their methods by mathematical induction. It is worth noting that their analysis techniques can be used to analyze our methods, which will be considered in our future work.

#### 4. Numerical results

In this section, we apply the proposed schemes to two benchmark gradient flow models: the Cahn-Hilliard model for binary fluids and the molecular beam epitaxial (MBE) growth model. For convenience, the LEQRK schemes equipped with Gauss4th and DIRK4th are abbreviated respectively as LEQGRK and LEQDIRK, while their corresponding LEQRK-PC schemes with M prediction iteration are denoted by LEQGRK-PC-M and LEQDIRK-PC-M, respectively.

#### 4.1. Cahn-Hilliard model

We consider the Cahn-Hilliard model for immiscible binary fluids given as follows

$$\phi_t = \lambda \Delta (-\varepsilon^2 \Delta \phi + \phi^3 - \phi), \tag{4.1}$$

with the double-well bulk energy

$$F = \frac{\varepsilon^2}{2} \|\nabla \phi\|^2 + \frac{1}{4} \|\phi^2 - 1\|^2, \tag{4.2}$$

where  $\lambda$  is the mobility parameter and  $\varepsilon$  controls the interfacial thickness. If we introduce the auxiliary variable  $q = \frac{1}{2}(\phi^2 - 1 - \gamma)$ , where  $\gamma \ge 0$  is a constant [6], the energy functional (4.2) is rewritten into

$$\mathcal{F} = \frac{1}{2} \left( \phi, -\varepsilon^2 \Delta \phi + \gamma \phi \right) + \|q\|^2 - \frac{\gamma^2 + 2\gamma}{4} |\Omega|. \tag{4.3}$$

Then the Cahn-Hilliard equation (4.1) is equivalently to the following gradient flow system

$$\begin{cases} \phi_t = \lambda \Delta (-\varepsilon^2 \Delta \phi + \gamma \phi + 2q\phi), \\ q_t = \phi \phi_t, \end{cases}$$
(4.4)

which satisfies the following energy dissipation law

$$\frac{d\mathcal{F}}{dt} = -\lambda \left\| \nabla (-\varepsilon^2 \Delta \phi + \gamma \phi + 2q\phi) \right\|^2 \le 0. \tag{4.5}$$

Applying the LEQRK-PC scheme to system (4.4), we obtain

**Scheme 4.1.** Let  $b_i$ ,  $a_{ij}$   $(i, j = 1, \dots, s)$  be real numbers and  $c_i = \sum_{j=1}^{s} a_{ij}$ . For given  $(\phi^n, q^n)$  and  $\Phi_N(t_n + c_i \Delta t)$ ,  $Q_N(t_n + c_i \Delta t)$ ,  $\forall i$ , defined previously, the following intermediate values are first calculated by the following prediction-correction step.

1. Prediction: we set  $\Phi_i^{n,0} = \Phi_N(t_n + c_i \Delta t)$ ,  $Q_i^{n,0} = Q_N(t_n + c_i \Delta t)$  and M > 0 as a given positive integer. For m = 0 to M - 1, we compute  $\Phi_i^{n,m+1}$ ,  $k_i^{n,m+1}$ ,  $l_i^{n,m+1}$ ,  $Q_i^{n,m+1}$  using

$$\begin{cases} \Phi_{i}^{n,m+1} = \phi^{n} + \Delta t \sum_{j=1}^{s} a_{ij} k_{j}^{n,m+1}, \\ k_{i}^{n,m+1} = \lambda \Delta \left( -\varepsilon^{2} \Delta \Phi_{i}^{n,m+1} + \gamma \Phi_{i}^{n,m+1} + 2 Q_{i}^{n,m} \Phi_{i}^{n,m} \right), \\ l_{i}^{n,m+1} = \Phi_{i}^{n,m+1} k_{i}^{n,m+1}, \\ Q_{i}^{n,m+1} = q^{n} + \Delta t \sum_{j=1}^{s} a_{ij} l_{j}^{n,m+1}, \end{cases}$$

$$(4.6)$$

Given an error tolerance TOL > 0, if  $\max_i \|\Phi_i^{n,m+1} - \Phi_i^{n,m}\|_{\infty} < TOL$ , we stop the iteration and set  $\Phi_i^{n,*} = \Phi_i^{n,m+1}$ ; otherwise, we set  $\Phi_i^{n,*} = \Phi_i^{n,M}$ .

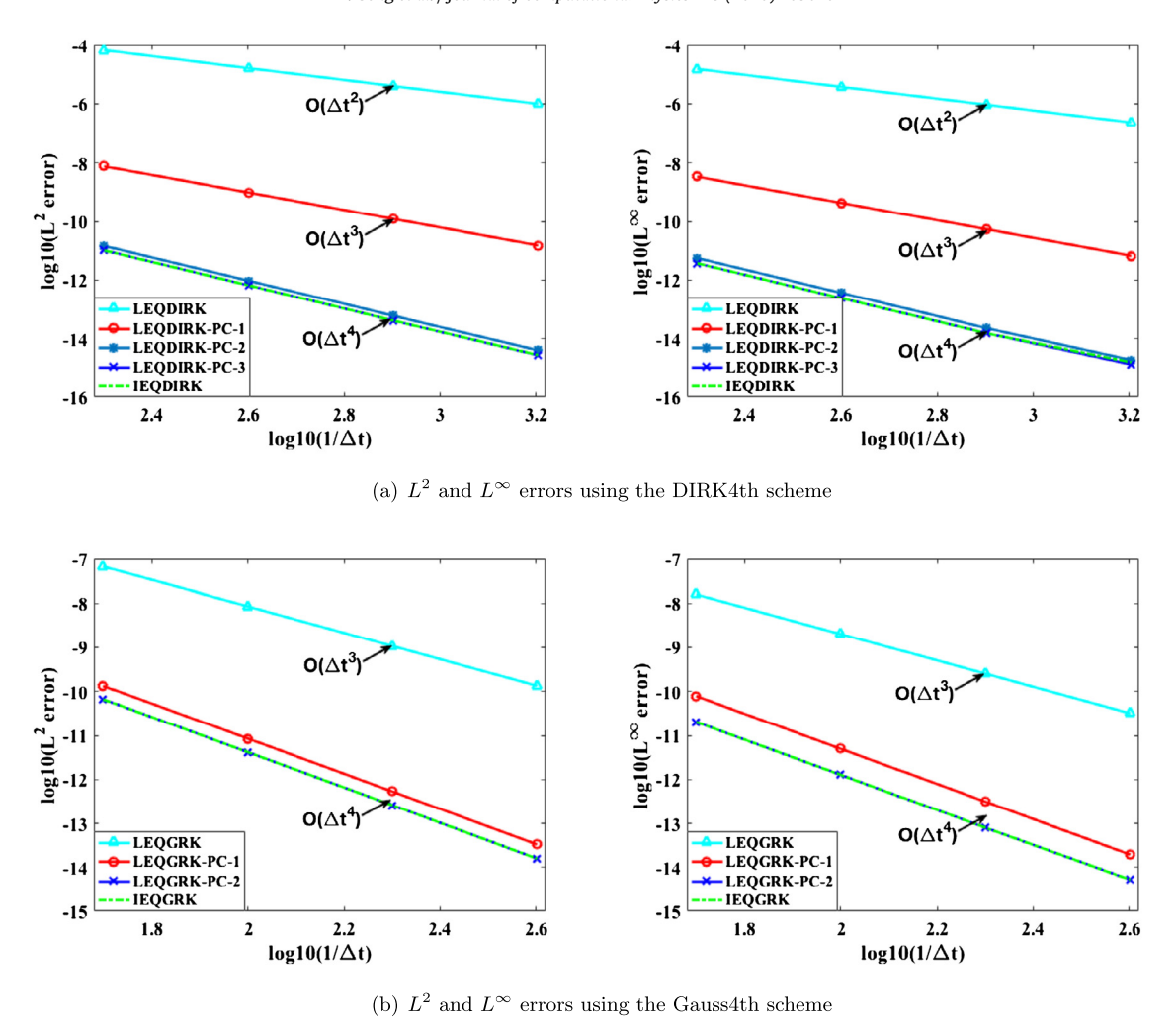


Fig. 4.1. Mesh refinement tests in time with the proposed numerical schemes LEQDIRK, LEQGRK, LEQDIRK-PC-M, LEQGRK-PC-M, M = 1, 2, 3, IEQDIRK and LEQGRK for the Cahn-Hilliard equation.

2. Correction: for the predicted  $\Phi_i^{n,*}$  obtained from the prediction step, we compute the intermediate values  $\Phi_i^n$ ,  $Q_i^n$ ,  $k_i^n$ ,  $l_i^n$  via

$$\begin{cases} \Phi_{i}^{n} = \phi^{n} + \Delta t \sum_{j=1}^{s} a_{ij} k_{j}^{n}, \\ Q_{i}^{n} = q^{n} + \Delta t \sum_{j=1}^{s} a_{ij} l_{j}^{n}, \\ k_{i}^{n} = \lambda \Delta \left( -\varepsilon^{2} \Delta \Phi_{i}^{n} + \gamma \Phi_{i}^{n} + 2 Q_{i}^{n} \Phi_{i}^{n,*} \right), \\ l_{i}^{n} = \Phi_{i}^{n,*} k_{i}^{n}, \end{cases}$$

$$(4.7)$$

Then  $(\phi^{n+1}, q^{n+1})$  is updated via

$$\phi^{n+1} = \phi^n + \Delta t \sum_{i=1}^s b_i k_i^n, \tag{4.8}$$

$$q^{n+1} = q^n + \Delta t \sum_{i=1}^s b_i l_i^n. (4.9)$$

First of all, we present mesh refinement tests in time to show the temporal order of accuracy of the proposed schemes. We consider the domain as  $[0 \ 2\pi]^2$  and choose model parameter values  $\lambda = 0.01$ ,  $\varepsilon = 1$  and  $\gamma = 1$ . Note that the analytical

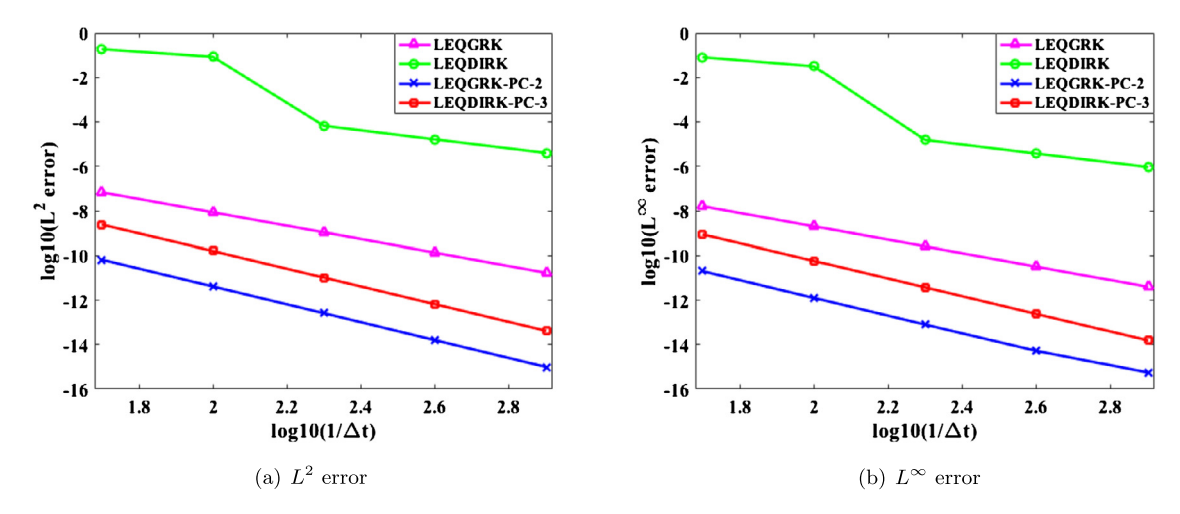


**Fig. 4.2.**  $L^2$  and  $L^\infty$  errors using DIRK4th and Gauss4th schemes for the Cahn-Hilliard equation.

solution of the Cahn-Hilliard equation is usually unknown. To better calculate the errors in mesh refinement tests in time, we create an exact solution  $\phi(x, y, t) = \sin(x)\sin(y)\cos(t)$ , by adding a corresponding forcing term on the right-hand side of the Cahn-Hilliard equation. Then, we solve it in a 2D spatial domain with periodic boundary conditions. The equation is discretized spatially using the Fourier pseudo-spectral method with 128<sup>2</sup> spatial meshes.

The numerical solution of  $\phi$  at t=1 is calculated using a set of different numerical schemes with various time steps. Both the  $L^2$  and  $L^\infty$  errors in the solution are calculated, and the results are summarized in Fig. 4.1. We observe that, due to the low-order extrapolation, LEQDIRK only reaches second-order accuracy, but it can reach the 4th order accuracy with only two prediction iterations. Similarly, due to the low-order extrapolation, LEQGRK only has the 3rd order accuracy, however it can easily reach the 4th order accuracy with one prediction iteration. From Fig. 4.1, we also see that the LEQDIRK-PC scheme with only three prediction iterations can reach similar accuracy as IEQDIRK proposed in [20], while the LEQGRK-PC scheme only requires two prediction iterations.

To further compare the DIRK4th and Gauss4th schemes, we summarize their  $L^2$  and  $L^\infty$  errors in Fig. 4.2(a)-(b), respectively. We observe that the Gauss4th scheme reaches its order of accuracy even with a larger time step size. After a few iterations, the DIRK4th scheme also reaches its order of accuracy quickly. Also, with the same time step size, the Gauss4th scheme is more accurate than the DIRK4th scheme.

To further benchmark these two schemes, we conduct several numerical tests. For comparison, we also implement the widely used second-order convex splitting scheme (which we refer to as the 2nd-CS scheme in this paper),

$$\frac{\phi^{n+1} - \phi^n}{\Delta t} = \lambda \Delta \left[ -\varepsilon^2 \Delta \phi^{n+\frac{1}{2}} + \frac{1}{2} ((\phi^n)^2 + (\phi^{n+1})^2) \phi^{n+\frac{1}{2}} - (\frac{3}{2} \phi^n - \frac{1}{2} \phi^{n-1}) \right]. \tag{4.10}$$

We note that there is no theoretical proof on energy dissipation for the 2nd-CS scheme above although it is more accurate than the first-order convex splitting scheme.

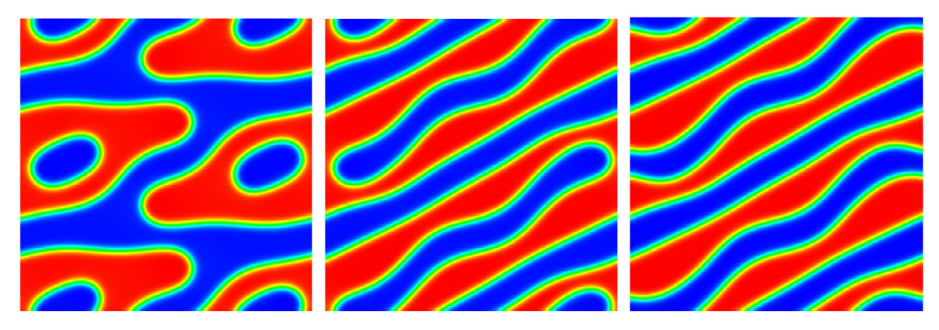
For the first example, we choose the domain as  $[0\ 1]^2$ , and parameters  $\lambda = 1$ ,  $\epsilon = 0.01$ , and  $\gamma = 1$ . Then, we use the initial condition

$$\phi(x, y, t = 0) = 0.05 \Big(\cos(3X)\cos(4Y) + (\cos(4X)\cos(3Y))^2 + \cos(X - 5Y)\cos(2X - Y)\Big), X = 2\pi x, Y = 2\pi y.$$
(4.11)

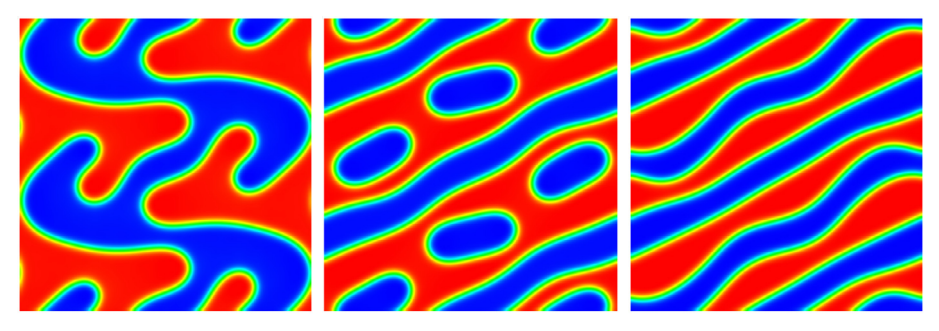
This initial profile initiates a fast coarsening dynamics such that an algorithm can predict 'wrong' dynamics if it is not accurate nor robust enough. In this example, we intend to find the maximum possible time step that one can capture the correct dynamics numerically, for which various numerical schemes with different time steps are implemented and compared. Note in this example that we set  $\Phi_i^{n,0} = \phi^n$ , and  $Q_i^{n,0} = q^n$  in the prediction step, instead of using interpolation values, as explained in Remark 3.6.

The numerical results are summarized in Fig. 4.3, where the predicted profile of  $\phi(x,y)$  at t=0.1 are shown using different schemes and time-step sizes. We observe that the maximum possible time step for the 2nd-order convex splitting scheme is approximately  $\Delta t = 6.25 \times 10^{-5}$ . For the DIRK4th scheme with 5 prediction iterations, the maximum time step is approximately  $\Delta t = 1.25 \times 10^{-4}$ . For the Gauss4th method with five prediction iterations, it is  $2.5 \times 10^{-4}$ . Notice that the prediction steps can be easily solved with FFT so that the computational cost is negligible compared to the correction step.

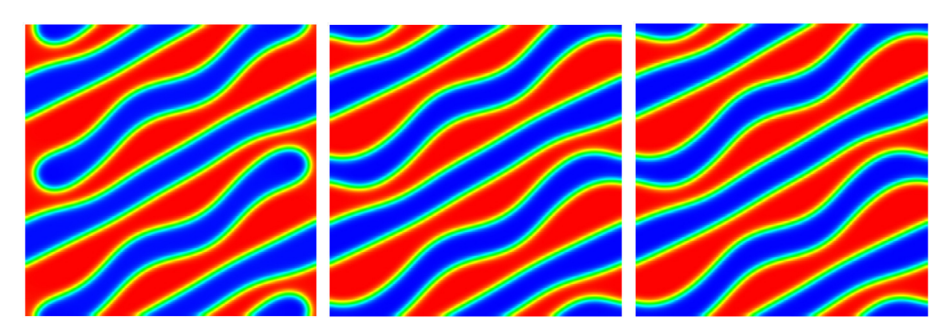
These results indicate that the DIRK4th and Gauss4th schemes are superior over the second-order convex splitting scheme in this simulation. In addition, one should notice that there is no theoretical guarantee of monotonic energy decay



(a) The profile of  $\phi$  at t=0.1 using various time step sizes:  $\Delta t=2.5\times 10^{-4}, 1.25\times 10^{-4}, 6.25\times 10^{-5}$  with the 2nd-order convex splitting scheme.



(b) The profile of  $\phi$  at t=0.1 using various time step sizes:  $\Delta t=5\times 10^{-4}, 2.5\times 10^{-4}, 1.25\times 10^{-4}$  with the DIRK4th scheme.



(c) The profile of  $\phi$  at t=0.1 using various time step sizes:  $\Delta t=5\times 10^{-4}, 2.5\times 10^{-4}, 1.25\times 10^{-4}$  with the Gauss4th scheme.

**Fig. 4.3.** A comparison of three schemes on predicting accurate Cahn-Hilliard dynamics at various time steps. The figures show the numerical results of  $\phi$  at time t = 0.1 using the three different schemes with various time steps. The last sub-figure in each row indicates the maximum possible time step size to predict the correct dynamics for the corresponding scheme. Both the DIRK4th scheme and the Gauss4th scheme perform better than the second-order CS scheme.

with the second-order convex splitting scheme, and the implementation of the convex splitting scheme is relatively complicated, as nonlinear equations have to be solved at each time step. In contrast, the proposed high-order schemes here are linear and easy to implement. Also, they are rather general so that they can be applied to a broad class of gradient flow models.

The calculated energies using different time steps for the numerical example in Fig. 4.3 are summarized in Fig. 4.4. We observe that all the calculated energies are decreasing with time although the numerical schemes with large time steps may not be accurate. They confirm the theoretical results that the proposed linear high-order schemes are unconditionally energy stable.

Next, we conduct an additional numerical experiment with random initial conditions for the same model. Specifically, we use

$$\phi(x, y, t = 0) = 0.001 \text{ rand}(x, y),$$

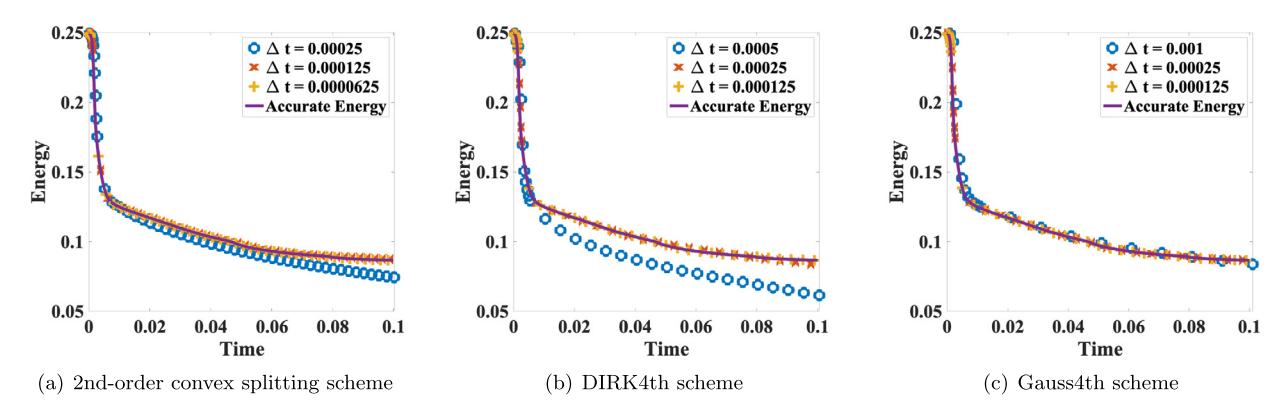


Fig. 4.4. Numerical energy evolution in time with respect to different time steps. This figures show the energies using different schemes with various time steps.

where rand(x, y) generates random numbers between -1 and 1 uniformly. The rest settings are kept the same as in the previous example. The numerical results are summarized in Fig. 4.5. This numerical example again shows that the new schemes allow larger steps for accurately predicting coarsening dynamics over the 2nd CS scheme.

#### 4.2. Molecular beam epitaxial growth model

To further test the newly proposed high order schemes, we use them to compute two molecular beam epitaxial (MBE) growth models: 1) the MBE model with slope selection is given as follows

$$\phi_t = -\lambda \left( \varepsilon^2 \Delta^2 \phi - \nabla \cdot \left( (|\nabla \phi|^2 - 1) \nabla \phi \right) \right), \tag{4.13}$$

where the free energy functional is given by

$$F = \frac{\varepsilon^2}{2} \|\Delta\phi\|^2 + \frac{1}{4} \||\nabla\phi|^2 - 1\|^2; \tag{4.14}$$

and 2) the MBE model without slope selection is given as follows

$$\phi_t = -\lambda \left( \varepsilon^2 \Delta^2 \phi + \nabla \cdot \left( \frac{1}{1 + |\nabla \phi|^2} \nabla \phi \right) \right),\tag{4.15}$$

where the free energy functional is given by

$$F = \frac{\varepsilon^2}{2} \|\Delta\phi\|^2 - \frac{1}{2} \ln(1 + |\nabla\phi|^2). \tag{4.16}$$

Given the two MBE models are similar, we only present the discrete scheme for the MBE model with slope selection in (4.13). The discrete scheme for the MBE model without slope selection in (4.15) could be derived similarly.

We define  $q = \frac{1}{2}(|\nabla \phi|^2 - 1 - \gamma)$  and rewrite the energy functional (4.14) as a quadratic functional

$$\mathcal{F} = \frac{1}{2} \left( \phi, \varepsilon^2 \Delta^2 \phi - \gamma \Delta \phi \right) + \|q\|^2 - \frac{\gamma^2 + 2\gamma}{4} |\Omega|. \tag{4.17}$$

Using the EQ reformulation, we have the following equivalent system

$$\begin{cases} \phi_t = -\lambda \Big( \varepsilon^2 \Delta^2 \phi - \gamma \Delta \phi - \nabla \cdot (2q \nabla \phi) \Big), \\ q_t = \nabla \phi \cdot \nabla \phi_t, \end{cases}$$
(4.18)

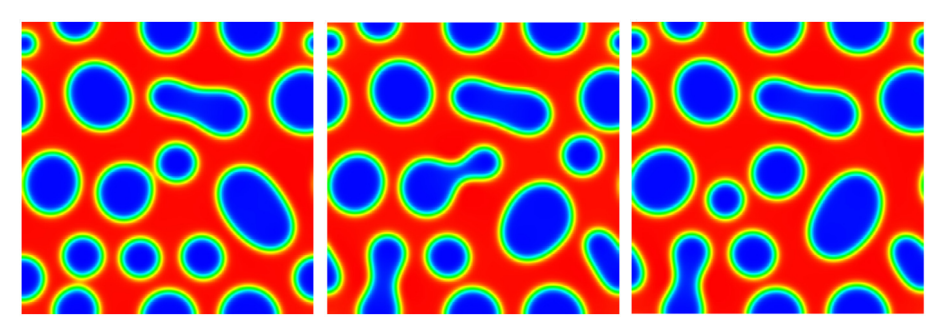
with the consistent initial condition

$$\begin{cases} \phi(t=0) = \phi_0, \\ q(t=0) = \frac{1}{2} (|\nabla \phi_0|^2 - 1 - \gamma). \end{cases}$$
(4.19)

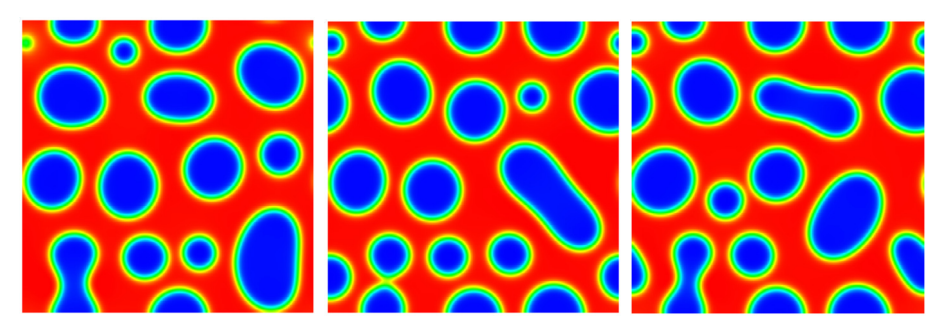
System (4.18) obeys the following energy dissipation law

$$\frac{d\mathcal{F}}{dt} = -\lambda \left\| \varepsilon^2 \Delta^2 \phi - \gamma \Delta \phi - \nabla \cdot (2q \nabla \phi) \right\|^2 \le 0. \tag{4.20}$$

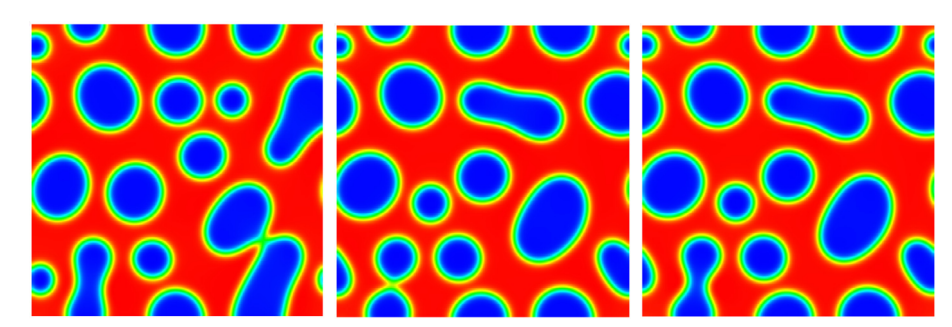
Applying the LEQRK-PC scheme to system (4.18), we have the following scheme specifically for this model.



(a) The profile of  $\phi$  at t=0.1 using various time steps:  $\Delta t=2.5\times 10^{-4}, 1.25\times 10^{-4}, 6.25\times 10^{-5}$  with the second-order convex splitting method



(b) The profile of  $\phi$  at t=0.1 using various time steps:  $\Delta t=5\times 10^{-4}, 2.5\times 10^{-4}, 1.25\times 10^{-5}$  with the DIRK4th method.



(c) The profile of  $\phi$  at t=0.1 using various time steps:  $\Delta t=5\times 10^{-4}, 2.5\times 10^{-4}, 1.25\times 10^{-5}$  with the Gauss4th method.

**Fig. 4.5.** A comparison of the three schemes on predicting accurate Cahn-Hilliard dynamics with random initial conditions. These figures show the numerical results of  $\phi$  at time t = 0.1 using different schemes with various time steps. The last sub-figure in each row indicates the maximum possible time step to predict correct dynamics with the corresponding scheme. The Gauss4th scheme performs the best.

**Scheme 4.2.** Let  $b_i$ ,  $a_{ij}$   $(i, j = 1, \dots, s)$  be real numbers and let  $c_i = \sum_{j=1}^s a_{ij}$ . For given  $(\phi^n, q^n)$  and  $\Phi_N(t_n + c_i \Delta t)$ ,  $Q_N(t_n + c_i \Delta t)$ ,  $\forall i$ , the following intermediate values are first calculated by the following prediction-correction strategy

1. Prediction: we set  $\Phi_i^{n,0} = \Phi_N(t_n + c_i \Delta t)$ ,  $Q_i^{n,0} = Q_N(t_n + c_i \Delta t)$  and M > 0 as a given integer. For m = 0 to M - 1, we compute  $\Phi_i^{n,m+1}$ ,  $k_i^{n,m+1}$ ,  $l_i^{n,m+1}$ ,  $Q_i^{n,m+1}$  using

$$\begin{cases} \Phi_{i}^{n,m+1} = \phi^{n} + \Delta t \sum_{j=1}^{s} a_{ij} k_{j}^{n,m+1}, \\ k_{i}^{n,m+1} = -\lambda \left( \varepsilon^{2} \Delta^{2} \Phi_{i}^{n,m+1} - \gamma \Delta \Phi_{i}^{n,m+1} - \nabla \cdot \left( 2 Q_{i}^{n,m} \nabla \Phi_{i}^{n,m} \right) \right), \\ l_{i}^{n,m+1} = \nabla \Phi_{i}^{n,m+1} \cdot \nabla k_{i}^{n,m+1}, \\ Q_{i}^{n,m+1} = q^{n} + \Delta t \sum_{j=1}^{s} a_{ij} l_{j}^{n,m+1}, \end{cases}$$

$$(4.21)$$

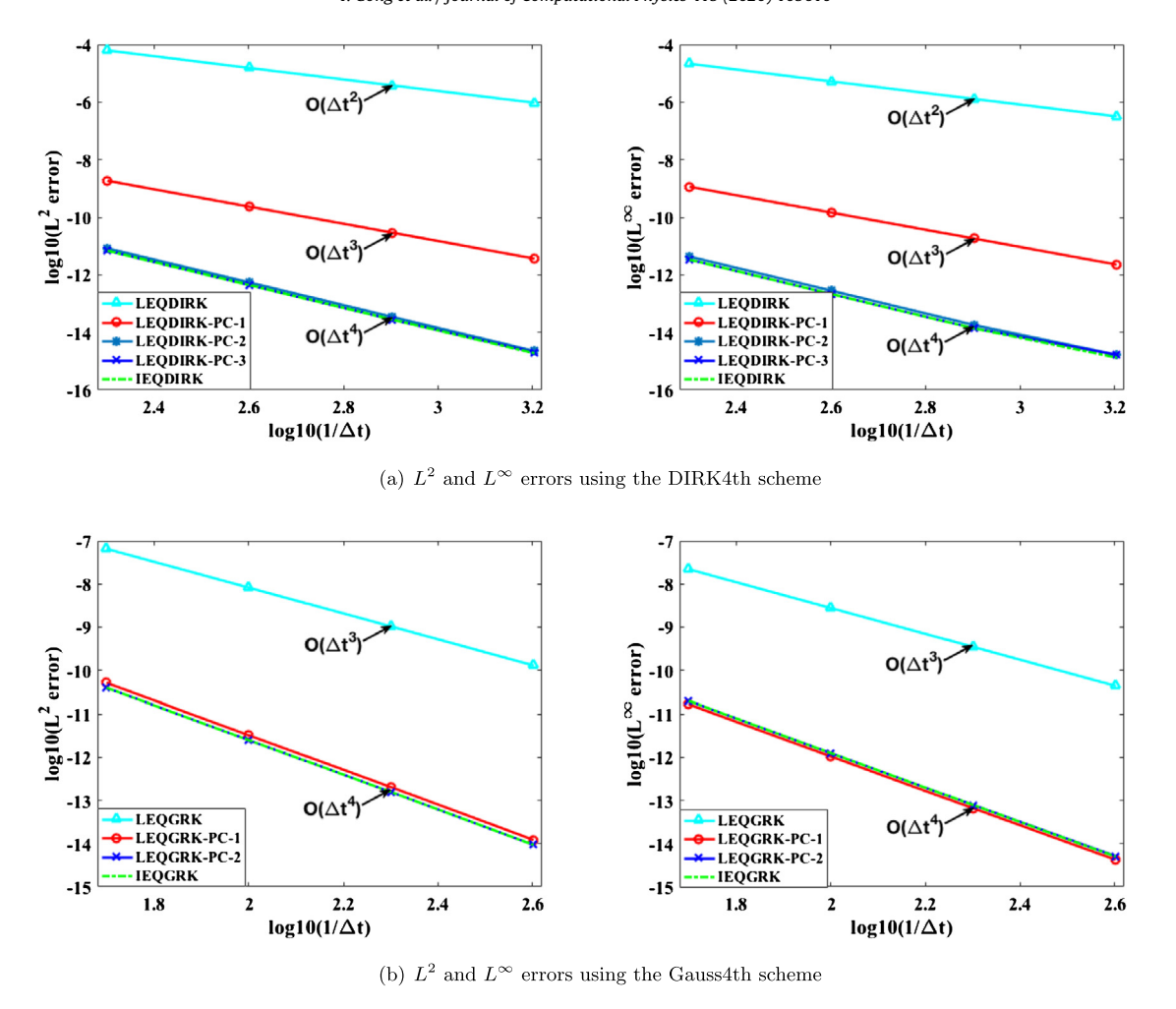


Fig. 4.6. Mesh refinement tests in time with the proposed numerical schemes for the MBE model with slope selection. The desired order of accuracy is reached with sufficient number of prediction iterations.

Given the error tolerance TOL>0, if  $\max_i \|\Phi_i^{n,m+1}-\Phi_i^{n,m}\|_\infty < TOL$ , we stop the iteration and set  $\Phi_i^{n,*}=\Phi_i^{n,m+1}$ ; otherwise, we set  $\Phi_i^{n,*} = \Phi_i^{n,M}$ . 2. Correction: for the predicted  $\Phi_i^{n,*}$ , we compute the intermediate values  $\Phi_i^n$ ,  $Q_i^n$ ,  $k_i^n$ ,  $l_i^n$  via

$$\begin{cases}
\Phi_{i}^{n} = \phi^{n} + \Delta t \sum_{j=1}^{s} a_{ij} k_{j}^{n}, \\
Q_{i}^{n} = q^{n} + \Delta t \sum_{j=1}^{s} a_{ij} l_{j}^{n}, \\
k_{i}^{n} = -\lambda \left( \varepsilon^{2} \Delta^{2} \Phi_{i}^{n} - \gamma \Delta \Phi_{i}^{n} - \nabla \cdot \left( 2 Q_{i}^{n} \nabla \Phi_{i}^{n,*} \right) \right), \\
l_{i}^{n} = \nabla \Phi_{i}^{n,*} \cdot \nabla k_{i}^{n},
\end{cases}$$

$$(4.22)$$

Then  $(\phi^{n+1}, q^{n+1})$  is updated via

$$\phi^{n+1} = \phi^n + \Delta t \sum_{i=1}^s b_i k_i^n, \tag{4.23}$$

$$q^{n+1} = q^n + \Delta t \sum_{i=1}^s b_i l_i^n. \tag{4.24}$$

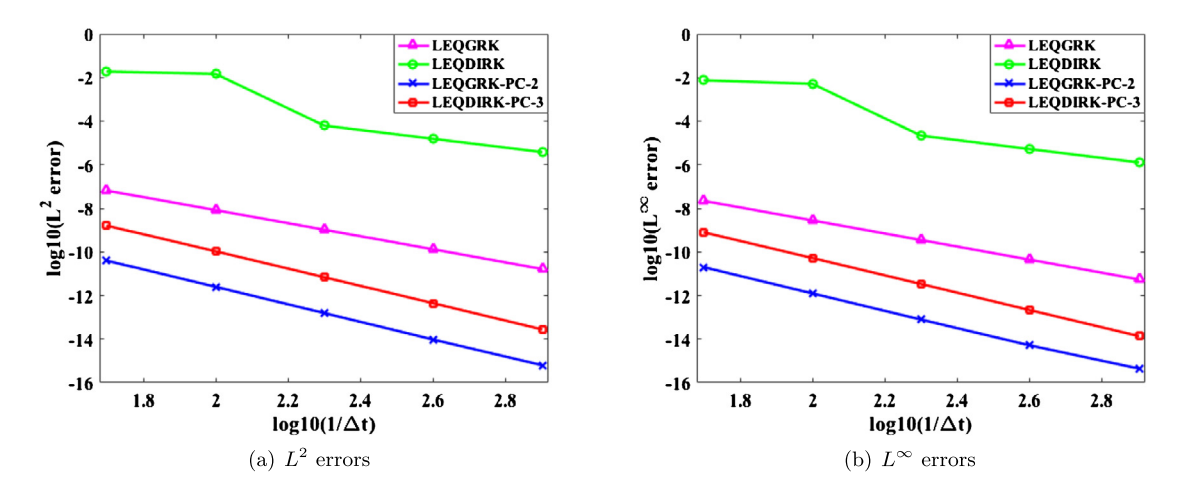


Fig. 4.7.  $L^2$  and  $L^\infty$  errors using the DIRK4th method and the Gauss4th method for the MBE model, respectively.

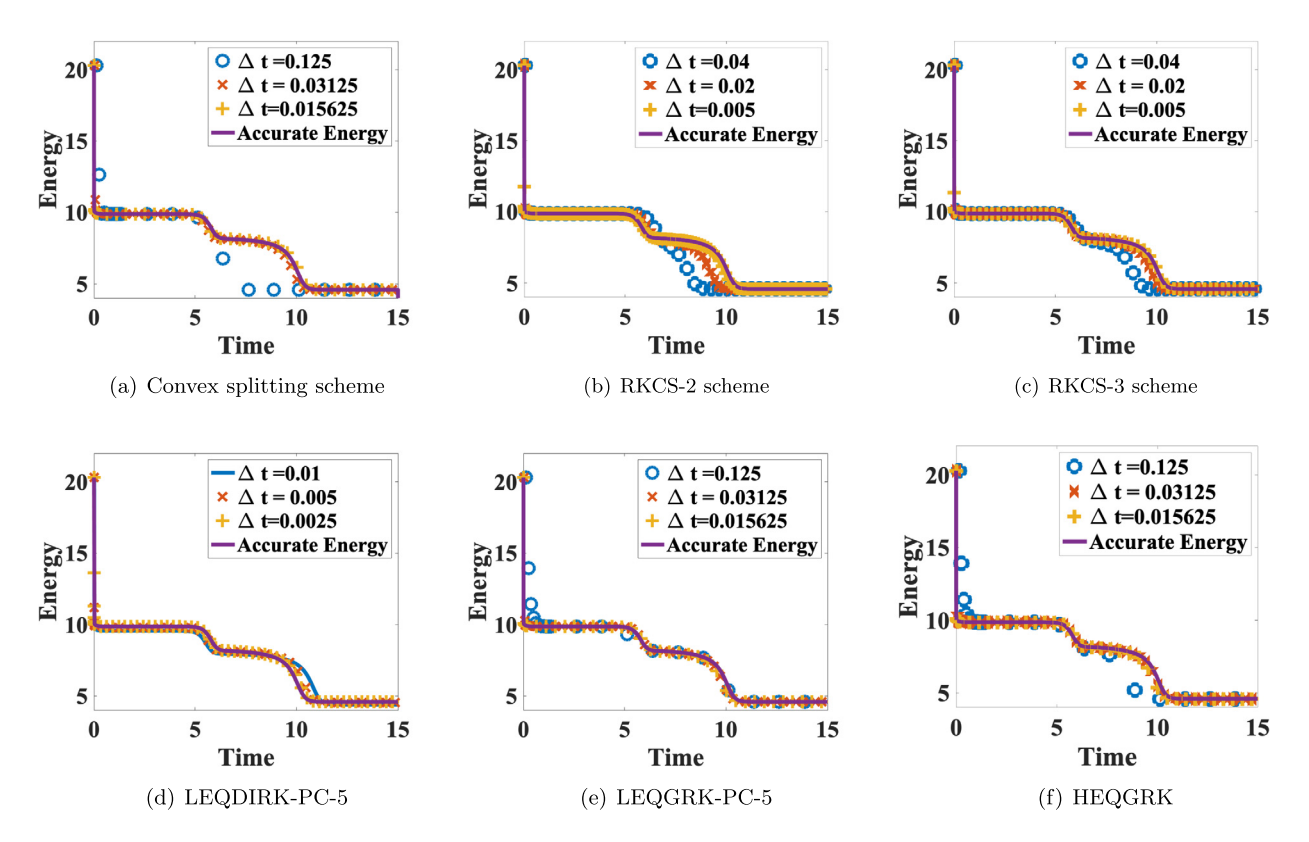
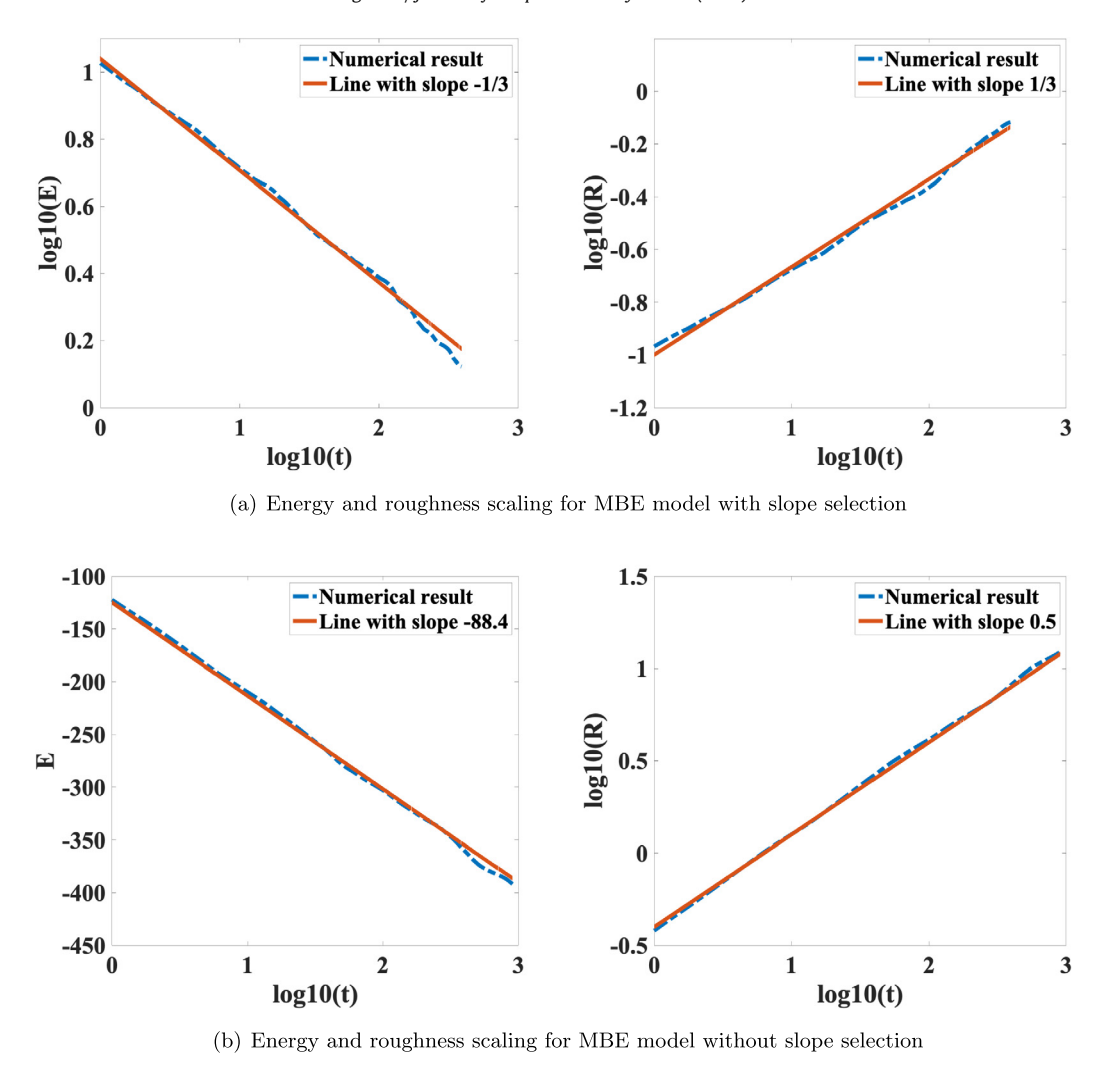


Fig. 4.8. Numerical results of energy evolution for the MBE model using different schemes with various time steps. Large time steps can be used in LEQGRK-PC-5 and HEQGRK.

We apply the scheme to solve the MBE model with slope selection given by Eq. (4.13). We repeat the mesh refinement test in time first, using domain  $[0\ 2\pi]^2$  and parameters  $\lambda=0.01$ ,  $\gamma=1$  and  $\varepsilon=1$ . By adding the proper force term on the right-hand side of the equation, we create an exact solution

$$\phi(x, y, t) = \sin(x)\sin(y)\cos(t), \tag{4.25}$$

for the MBE model with slope selection and the added forcing term. Then, we solve the modified model equation in the domain with a periodic boundary condition using the pseudo-spectral method for spatial discretization on  $128^2$  meshes. The  $L^2$  errors and  $L^\infty$  errors using different schemes and various time steps are summarized in Fig. 4.6. Here, we observe similar results, i.e., the DIRK4th scheme reaches second-order accuracy without the prediction, but obtain 4th order accuracy with only two iteration steps in the prediction step for both the  $L^2$  and  $L^\infty$  norms. This is due to the low-order approximation



**Fig. 4.9.** Numerical results show proper power law dynamics for both MBE models. (a) For the MBE model with slope selection, the energy decreases as  $O(t^{-1/3})$  and the roughness increases as  $O(t^{1/3})$ . (b) For the MBE model without slope selection, the energy decreases as  $O(-88.4\log(t))$  and the roughness increases as  $O(t^{1/2})$ . Here E represent the energy and R the roughness [44].

for extrapolating the explicit terms. Analogously, the Gauss4th scheme is 3rd order accurate without any prediction steps and reaches 4th order accuracy with one iteration step.

To compare the accuracy of the DIRK4th scheme with that of the Gauss4th scheme in solving the MBE model with slope selection, we summarize their  $L^2$  and  $L^\infty$  errors in 4.7. We observe that the Gauss4th method yields a smaller error than the DIRK4th scheme if using the same time step.

Next, we conduct a comparative study using the proposed DIRK4th and Gauss4th schemes and a second order convex splitting scheme for the MBE model with slope selection given in Eq. (4.13). The 2nd-order convex splitting scheme (2nd order CS) is given by

$$\frac{\phi^{n+1} - \phi^n}{\delta t} = -\lambda \left( \varepsilon^2 \Delta^2 \phi^{n+\frac{1}{2}} - \frac{1}{2} \nabla \cdot \left( (|\nabla \phi^{n+1}|^2 + |\nabla \phi^n|^2) \nabla \phi^{n+\frac{1}{2}} \right) + \Delta \left( \frac{3}{2} \phi^n - \frac{1}{2} \phi^{n-1} \right) \right). \tag{4.26}$$

Also, we compare our proposed schemes with the second-order and third-order convex splitting Runge-Kutta schemes given in [42], referred as RKCS2 and RKCS3 respectively. Note that we set  $\Phi_i^{n,0} = \phi^n$ , and  $Q_i^{n,0} = q^n$  in the prediction step, instead of using interpolation values, as explained in Remark 3.6.

Following [44], we choose the domain as  $[0\ 2\pi]^2$ , parameters  $\lambda=1$ ,  $\varepsilon^2=0.1$ , and  $\gamma=1$ . We solve the MBE model in a periodic domain using the pseudo-spectral method with  $128^2$  meshes. All the numerical schemes (i.e., the DIRK4th, Gauss4th, 2nd order CS scheme, RKCS2, and RKCS3) are implemented. Five prediction iterations are used for both the DIRK4th and Gauss4th scheme. The energy from t=0 to t=15 are calculated with different time steps and the results are summarized in Fig. 4.8. We observe that the maximum time step to obtain accurate solutions is  $\Delta t=0.015625$  for

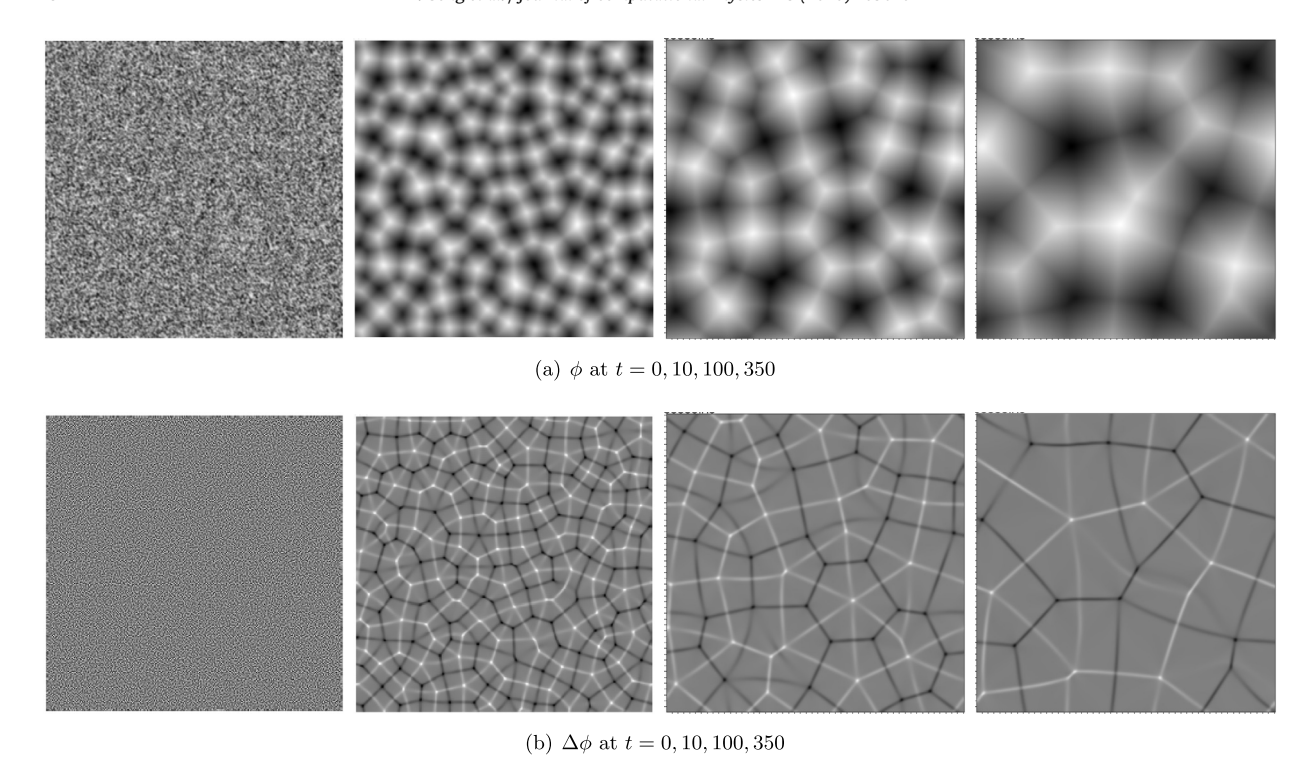


**Fig. 4.10.** The profile of  $\phi$  and  $\Delta \phi$  at different times for the MBE model with slope selection.

the second-order convex splitting scheme,  $\Delta t = 0.01$  for RKCS-3,  $\Delta t = 0.0025$  for LEQDIRK-PC-5, and  $\Delta t = 0.015625$  for LEQGRK-PC-5, respectively. We also implemented the fully implicit Gauss4th scheme proposed in our previous work [24], named as HEQGRK, and plot the results in Fig. 4.8(f). By comparing results in Fig. 4.8(e) and those in Fig. 4.8(f), we observe that the accuracy of the proposed arbitrarily high order linear schemes with prediction steps is comparable to the arbitrarily high-order, fully implicit schemes developed in our previous work [24]. For the newly proposed linear schemes, however, the complexity in numerical implementation and the computational cost are much reduced. In addition, we note that nonlinear equations have to be solved at each time step in the 2nd-order convex splitting scheme (4.26) or the RKCS2 or RKCS3 in [42] implemented for the MBE model. In comparison, the proposed schemes in this paper are all linear and easy to implement.

With the proposed high-order schemes, we can easily solve the MBE model with relatively larger time steps in most cases, making simulating long-time dynamics practical. Here we give an additional example as an illustration. We choose the domain as  $[0\ 12.8]^2$  and  $\varepsilon=0.03$ . The rest parameters are the same as in previous examples. We use  $256^2$  meshes. It is known that coarsening dynamics in the MBE model follows scaling laws [44]. For the MBE model with slope selection, the energy decreases as  $O(t^{-\frac{1}{3}})$ , and the roughness increases as  $O(t^{\frac{1}{3}})$  [44]. For the MBE model without slope selection, the energy decreases as  $O(-\log(t))$ , and the roughness increases as  $O(t^{\frac{1}{2}})$ . We implement our new schemes for both MBE models. The numerical results are summarized in Fig. 4.9, demonstrating a very good agreement with the expected scaling laws as [44].

The profile of  $\phi$  and  $\Delta \phi$  at different times for the MBE model with and without slope selections are summarized in Fig. 4.10 and 4.11, respectively. These profiles look qualitatively the same to the reported results, which strongly support our claim that the arbitrarily high order linear schemes can be applied to predict accurate dynamics for the MBE models.

#### 5. Conclusions

In this paper, we present a new paradigm for developing arbitrarily high order, fully discrete, linear numerical algorithms. These newly proposed algorithms have several advantageous properties: (1) the schemes are all linear so that they are easy to implement and computationally efficient; (2) the schemes are unconditionally energy stable and uniquely solvable such that large time steps can be used in long-time dynamical simulations; (3) the schemes can reach arbitrarily high-order of accuracy in both space and time so that relatively large meshes can guarantee the desired accuracy of numerical solutions; (4) the schemes do not depend on the specific expression of the free energy explicitly such that it can be readily applied to a large class of general gradient flow models. The proofs for energy stability and unique solvability for the general gradient flow models are given, and numerical tests with benchmark problems are shown to illustrate the usefulness and efficiency of the proposed schemes.

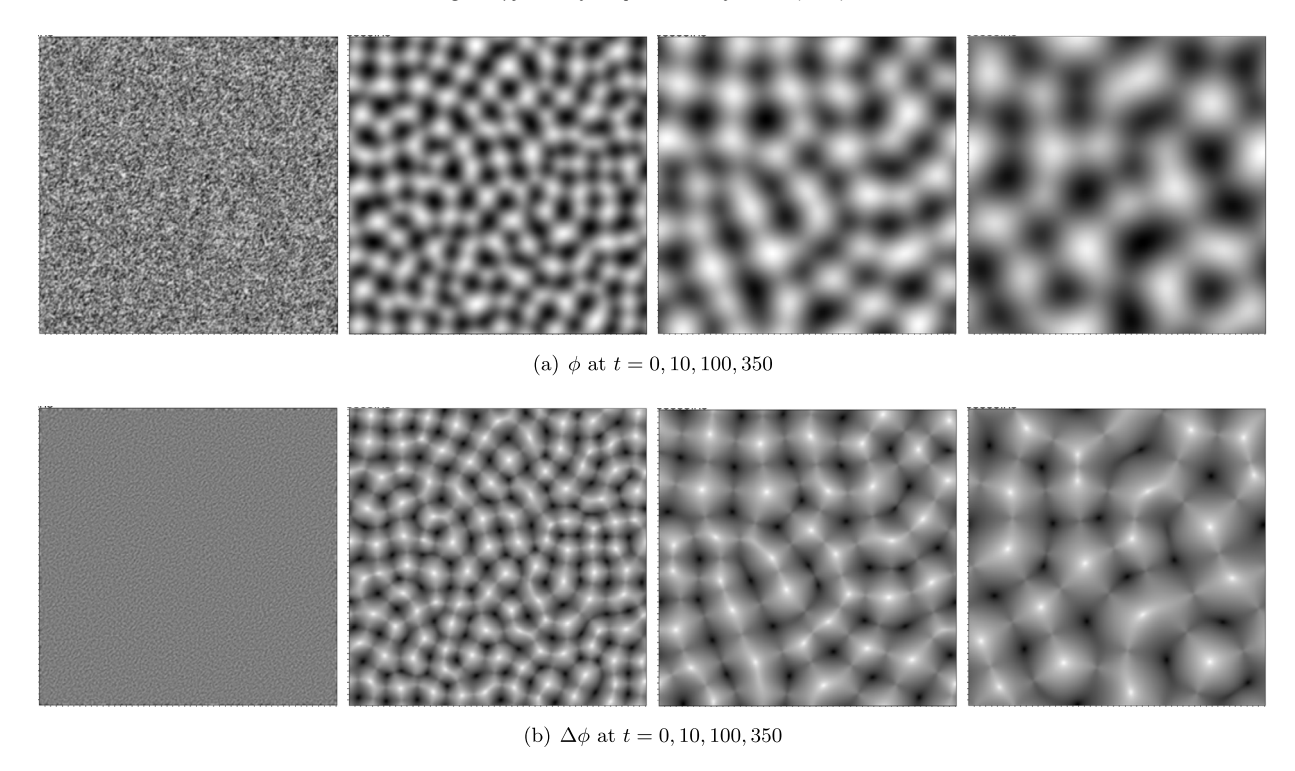


**Fig. 4.11.** The profile of  $\phi$  and  $\Delta \phi$  at different times for the MBE model without slope selection.

#### **Declaration of competing interest**

The authors declare that they have no known competing financial interests or personal relationships that could have appeared to influence the work reported in this paper.

## Acknowledgements

Yuezheng Gong's work is partially supported by the Foundation of Jiangsu Key Laboratory for Numerical Simulation of Large Scale Complex Systems (Grant No. 202002), the Natural Science Foundation of Jiangsu Province (Grant No. BK20180413) and the National Natural Science Foundation of China (Grant No. 11801269). Jia Zhao would like to acknowledge the support from NSF-DMS-1816783 and NVIDIA Corporation for the donation of a Quadro P6000 GPU for conducting some of the numerical simulations in this paper. Qi Wang's work is partially supported by NSF-DMS-1815921, OIA-1655740, a GEAR award from SC EPSCOR/IDeA Program and DE-SC0020272.

#### References

- [1] G. Akrivis, B. Li, D. Li, Energy-decaying extrapolated RK-SAV methods for the Allen-Cahn and Cahn-Hilliard equations, SIAM J. Sci. Comput. 41 (6) (2019) A3703–A3727.
- [2] J.W. Barrett, J.F. Blowey, H. Garcke, On fully practical finite element approximations of degenerate Cahn-Hilliard systems, ESAIM: M2AN 35 (2001) 713–748.
- [3] K. Burrage, J.C. Butcher, Stability criteria for implicit Runge-Kutta methods, SIAM J. Numer. Anal. 16 (1) (1979) 46-57.
- [4] J.W. Cahn, S.M. Allen, A microscopic theory for domain wall motion and its experimental verification in Fe-Al alloy domain growth kinetics, J. Phys., Colloq. 38 (C7) (1977) C7-51-C7-54.
- [5] J.W. Cahn, J.E. Hilliard, Free energy of a nonuniform system. I. Interfacial free energy, J. Chem. Phys. 28 (1958) 258-267.
- [6] L. Chen, J. Zhao, X. Yang, Regularized linear schemes for the molecular beam epitaxy model with slope selection, Appl. Numer. Math. 128 (2018) 138–156.
- [7] W. Chen, S. Conde, C. Wang, X. Wang, S. Wise, A linear energy stable scheme for a thin film model without slope selection, J. Sci. Comput. 52 (2012) 546–562.
- [8] K. Cheng, W. Feng, C. Wang, S. Wise, An energy stable fourth order finite difference scheme for the Cahn-Hilliard equation, J. Comput. Appl. Math. 362 (2019) 574–595.
- [9] K. Cheng, Z. Qiao, C. Wang, A third order exponential time differencing numerical scheme for no-slope-selection epitaxial thin film model with energy stability, J. Sci. Comput. 81 (1) (2019) 154–185.
- [10] K. Cheng, C. Wang, S. Wise, X. Yue, A second-order, weakly energy-stable pseudo-spectral scheme for the Cahn-Hilliard equation and its solution by the homogeneous linear iteration method, J. Sci. Comput. 69 (3) (2016) 1083–1114.
- [11] Q. Cheng, X. Yang, J. Shen, Efficient and accurate numerical schemes for a hydrodynamically coupled phase field diblock copolymer model, J. Comput. Phys. 341 (2017) 44–60.

- [12] S. Clarke, D.D. Vvedensky, Origin of reflection high-energy electron-diffraction intensity oscillations during molecular-beam epitaxy: a computational modeling approach, Phys. Rev. Lett. 58 (1987) 2235–2238.
- [13] A. Diegel, C. Wang, S. Wise, Stability and convergence of a second order mixed finite element method for the Cahn-Hilliard equation, IMA J. Numer. Anal. 36 (2016) 1867–1897.
- [14] S. Dong, Z. Yang, L. Lin, A family of second-order energy-stable schemes for Cahn-Hilliard type equations, J. Comput. Phys. 383 (2019) 24-54.
- [15] M. Elsey, B. Wirth, A simple and efficient scheme for phase field crystal simulation, ESAIM: M2AN 47 (2013) 1413-1432.
- [16] D. Eyre, Unconditionally gradient stable time marching the Cahn-Hilliard equation, in: Computational and Mathematical Models of Microstructural Evolution, San Francisco, CA, 1998, vol. 529, 1998, pp. 39–46.
- [17] W. Feng, C. Wang, S. Wise, Z. Zhang, A second-order energy stable backward differentiation formula method for the epitaxial thin film equation with slope selection, Numer. Methods Partial Differ. Equ. 34 (6) (2018) 1975–2007.
- [18] D. Furihata, T. Matsuo, Discrete Variational Derivative Method. A Structure-Preserving Numerical Method for Partial Differential Equations, CRC Press, 2011.
- [19] K. Glasner, S. Orizaga, Improving the accuracy of convexity splitting methods for gradient flow equations, J. Comput. Phys. 315 (2016) 52-64.
- [20] Y. Gong, J. Zhao, Energy-stable Runge-Kutta schemes for gradient flow models using the energy quadratization approach, Appl. Math. Lett. 94 (2019) 224–231.
- [21] Y. Gong, J. Zhao, Q. Wang, Linear second order in time energy stable schemes for hydrodynamic models of binary mixtures based on a spatially pseudospectral approximation, Adv. Comput. Math. 44 (2018) 1573–1600.
- [22] Y. Gong, J. Zhao, Q. Wang, Second order fully discrete energy stable methods on staggered grids for hydrodynamic phase field models of binary viscous fluids, SIAM J. Sci. Comput. 40 (2) (2018) B528–B553.
- [23] Y. Gong, J. Zhao, Q. Wang, Arbitrarily high-order unconditionally energy stable SAV schemes for gradient flow models, Comput. Phys. Commun. 249 (2020) 107033.
- [24] Y. Gong, J. Zhao, Q. Wang, Arbitrarily high-order unconditionally energy stable schemes for thermodynamically consistent gradient flow models, SIAM J. Sci. Comput. 42 (1) (2020) B135–B156.
- [25] F. Guillen-Gonzalez, G. Tierra, Second order schemes and time-step adaptivity for Allen-Cahn and Cahn-Hilliard models, Comput. Math. Appl. 68 (8) (2014) 821–846.
- [26] J. Guo, C. Wang, S. Wise, X. Yue, An  $h^2$  convergence of a second-order convex-splitting, finite difference scheme for the three-dimensional Cahn-Hilliard equation, Commun. Math. Sci. 14 (2) (2016) 489–515.
- [27] Z. Guo, P. Lin, J. Lowengrub, S. Wise, Mass conservative and energy stable finite difference methods for the quasi-incompressible Navier-Stokes-Cahn-Hilliard system: primitive variable and projection-type schemes, Comput. Methods Appl. Mech. Eng. 326 (2017) 144–174.
- [28] D. Hou, M. Azaiez, C. Xu, A variant of scalar auxiliary variable approaches for gradient flows, J. Comput. Phys. 395 (2019) 307-332.
- [29] W. Hu, M. lai, Unconditionally energy stable immersed boundary method with application to vesicle dynamics, East Asian J. Appl. Math. 3 (3) (2013) 247–262.
- [30] J. Kim, K. Kang, J. Lowengrub, Conservative multigrid methods for ternary Cahn-Hilliard systems, Commun. Math. Sci. 2 (2004) 53-77.
- [31] W. Li, W. Chen, C. Wang, Y. Yan, R. He, A second order energy stable linear scheme for a thin film model without slope selection, J. Sci. Comput. 76 (3) (2018) 1905–1937.
- [32] Z. Liu, X. Li, Efficient modified techniques of invariant energy quadratization approach for gradient flows, Appl. Math. Lett. 98 (2019) 206-214.
- [33] F. Luo, H. Xie, M. Xie, F. Xu, Adaptive time-stepping algorithms for molecular beam epitaxy: based on energy or roughness, Appl. Math. Lett. 99 (2020) 105991
- [34] Z. Qiao, Z. Sun, Z. Zhang, Stability and convergence of second-order schemes for the nonlinear epitaxial growth model without slope selection, Math. Comput. 84 (292) (2015) 653–674.
- [35] Z. Qiao, Z. Zhang, Tao Tang, An adaptive time-stepping strategy for the molecular beam epitaxy models, SIAM J. Sci. Comput. 33 (3) (2011) 1395-1414.
- [36] J. Shen, C. Wang, X. Wang, S. Wise, Second-order convex splitting schemes for gradient flows with Ehrlich-Schwoebel type energy: application to thin film epitaxy, SIAM J. Numer. Anal. 50 (1) (2012) 105–125.
- [37] J. Shen, J. Xu, Stabilized predictor-corrector schemes for gradient flows with strong anisotropic free energy, Commun. Comput. Phys. 24 (3) (2018) 635–654.
- [38] J. Shen, J. Xu, J. Yang, The scalar auxiliary variable (SAV) approach for gradient flows, J. Comput. Phys. 353 (2018) 407-416.
- [39] J. Shen, J. Xu, J. Yang, A new class of efficient and robust energy stable schemes for gradient flows, SIAM Rev. 61 (3) (2019) 474-506.
- [40] J. Shen, X. Yang, Numerical approximations of Allen-Cahn and Cahn-Hilliard equations, Discrete Contin. Dyn. Syst., Ser. A 28 (2010) 1669-1691.
- [41] J. Shin, H. Lee, J. Lee, Convex splitting Runge-Kutta methods for phase-field models, Comput. Math. Appl. 73 (2017) 2388-2403.
- [42] J. Shin, H. Lee, J. Lee, Unconditionally stable methods for gradient flow using convex splitting Runge-Kutta scheme, J. Comput. Phys. 347 (2017) 367–381.
- [43] C. Theng, I. Chern, M. Lai, Simulating binary fluid-surfactant dynamics by a phase field model, Discrete Contin. Dyn. Syst., Ser. B 17 (4) (2012) 1289–1307.
- [44] C. Wang, X. Wang, S. Wise, Unconditionally stable schemes for equations of thin film epitaxy, Discrete Contin. Dyn. Syst. 28 (1) (2010) 405-423.
- [45] S.-L. Wang, R.F. Sekerka, A.A. Wheeler, B.T. Murray, S.R. Coriell, R.J. Braun, G.B. McFadden, Thermodynamically-consistent phase-field models for solidification, Physica D 69 (1993) 189–200.
- [46] S. Wise, J. Kim, J. Lowengrub, Solving the regularized strongly anisotropic Cahn-Hilliard equation by an adaptive nonlinear multigrid method, J. Comput. Phys. 226 (1) (2007) 414–446.
- [47] S. Wise, C. Wang, J.S. Lowengrub, An energy-stable and convergent finite-difference scheme for the phase field crystal equation, SIAM J. Numer. Anal. 47 (3) (2009) 2269–2288.
- [48] Z. Xu, X. Yang, H. Zhang, Z. Xie, Efficient and linear schemes for anisotropic Cahn-Hilliard model using the stabilized-invariant energy quadratization (S-IEQ) approach, Comput. Phys. Commun. 238 (2019) 36–49.
- [49] Y. Yan, W. Chen, C. Wang, S. Wise, A second-order energy stable BDF numerical scheme for the Cahn-Hilliard equation, Commun. Comput. Phys. 23 (2) (2018) 572–602.
- [50] X. Yang, Linear, first and second-order, unconditionally energy stable numerical schemes for the phase field model of homopolymer blends, J. Comput. Phys. 327 (2016) 294–316.
- [51] X. Yang, L. Ju, Efficient linear schemes with unconditional energy stability for the phase field elastic bending energy model, J. Comput. Phys. 315 (2017) 691–712.
- [52] X. Yang, J. Zhao, Q. Wang, Numerical approximations for the molecular beam epitaxial growth model based on the invariant energy quadratization method, J. Comput. Phys. 333 (2017) 104–127.
- [53] X. Ye, The Legendre collocation method for the Cahn-Hilliard equation, J. Comput. Appl. Math. 150 (2003) 87-108.
- [54] Z. Zhang, Y. Ma, Z. Qiao, An adaptive time-stepping strategy for solving the phase field crystal model, J. Comput. Phys. 249 (2013) 204-215.
- [55] J. Zhao, X. Yang, Y. Gong, X. Zhao, J. Li, X. Yang, Q. Wang, A general strategy for numerical approximations of thermodynamically consistent nonequilibrium models-part I: thermodynamical systems, Int. J. Numer. Anal. Model. 15 (6) (2018) 884–918.